People's Democratic Republic of Algeria

Ministry of Higher Education and Scientific Research

Amar-Thelidji University - Laghouat

FACULTY OF TECHNOLOGY

DEPARTMENT OF ELECTRONICS

Master's Dissertation

Domain: Technology Sciences

Filiere: Electronics

Option: Instrumentation

Dissertation Topic

Design and Simulation of $CsSnGeI_3$ based-perovskite solar cells. Using SCAPS 1D

Presented by:

- **YOUSFI MOULAY ABDESSAMED**
- **DAKMOUSSI OMAR**

Publicly supported in front of the jury composed of:

Names	Grade	Quality
BIRANE Mouhoub	Prof	President
BENDELALA Fathi	MCA	Examiner
BELLAKHDAR Aissa	MCA	Supervisor

Promotion : 2025/2026

Dedication 1

بسم الله الرحمن الرحيم

Praise be to Allah at the beginning and at the end, for no path
is not covered, no effort is crowned with success and none quest does not succeed without His help.
Whoever says, "She is mine," shall have her; and if she refuses, I
will bring him by force.
Here I am today, taking the final steps of this
path, after years of effort and work devoted to the search for knowledge
O Allah, to You be praise until You are satisfied, and to You be the praise if You are satisfied
I also want to express my gratitude and my gratitude to those who gave me life, and I pray to Allah
Dear directors, professors, and specialized teachers, thank you
for your efforts; may Allah reward you.
And to our friends whom the school benches allowed us to meet and who have become like brothers for us,
Thank you.



2026

Y. MOULAY ABDESSAMED

Dedication

بسم الله الرحمن الرحيم

To my parents,

I dedicate this work to my parents, who have been my greatest support throughout my life and my main source of inspiration for success.

To my family, especially my siblings,

I sincerely thank you for your continuous support and encouragement. I hope to make you proud.

To my friends and colleagues,

Thank you for your support and for the memorable moments we shared, which helped me overcome difficulties.

To my teachers,

I sincerely appreciate your knowledge, guidance, and continuous support.

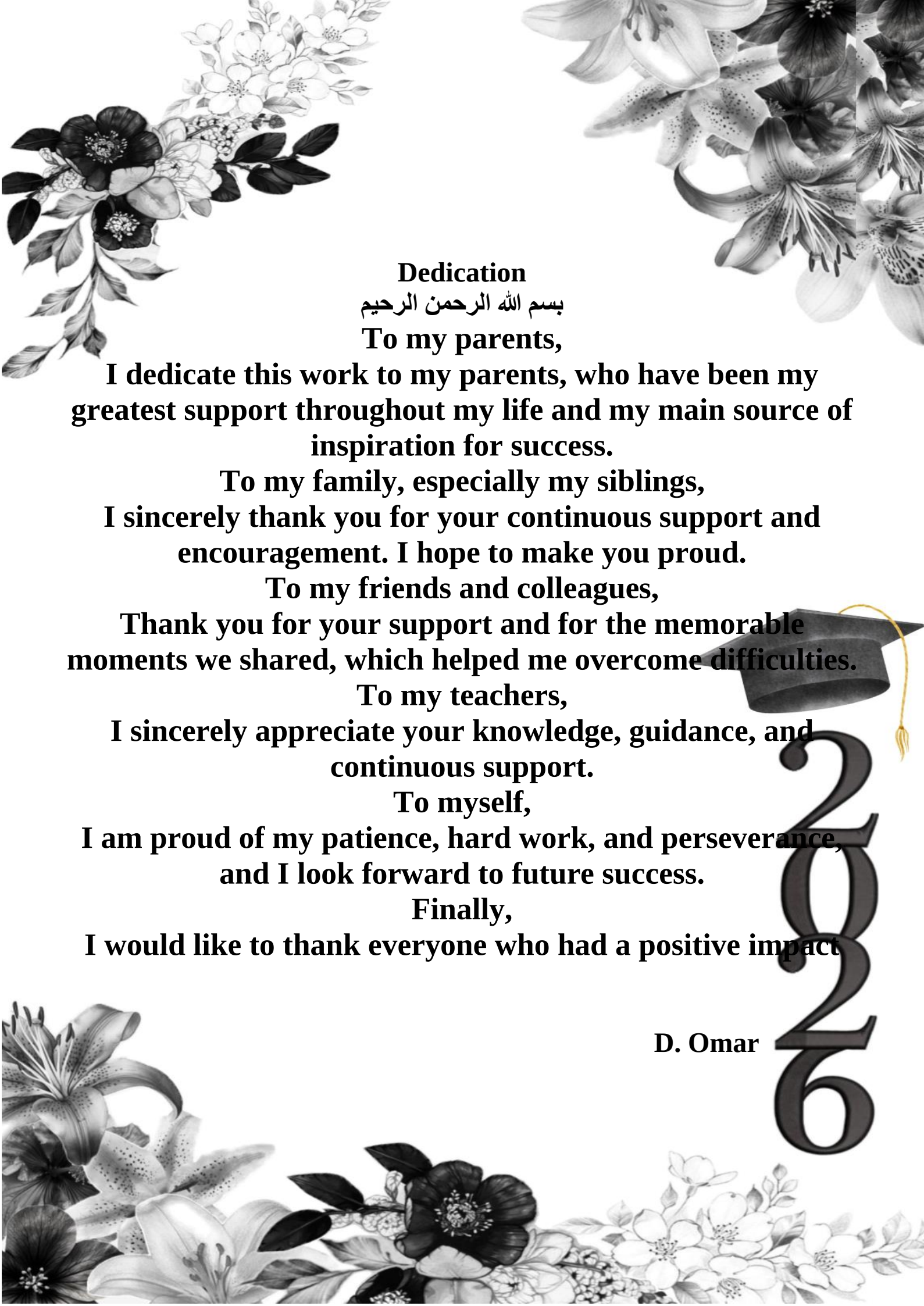
To myself,

I am proud of my patience, hard work, and perseverance, and I look forward to future success.

Finally,

I would like to thank everyone who had a positive impact

D. Omar



Remerciements:

First of all, we would like to express our deep thanks to Almighty Allah for the will, courage, health, and patience he has given us during these long years of study that we can reach this point.

Secondly, we express our deep gratitude to our coach **Dr. Aissa Bellakhdar**

for his enormous help, throughout the preparation of this thesis, also the jury members who agreed to judge this modest work.

Thus, our deep thanks also go to our dear parents, our dear brothers, for their contribution, their support and their patience.

Finally, we would like to thank all those who contributed directly or indirectly to the realization of this work.

Thank you all.

ABSTRACT

This Master's thesis studies lead-free perovskite solar cells based on the inorganic alloy $CsSnGeI_3$. It reviews photovoltaic fundamentals, presents the properties of perovskite materials, and uses SCAPS-1D simulations to optimize cell performance. The study identifies an absorber thickness of 1000 nm and the $CuSbS_2$/ZnO transport-layer combination as the best configuration, leading to a simulated efficiency of about 22.83%. It also shows that temperature and material defects strongly affect device stability and performance.

Keywords :Lead-free perovskite solar cells, $CsSnGeI_3$, SCAPS-1D simulation, solar cell optimization.

Résumé

Ce mémoire de Master étudie les cellules solaires à pérovskite sans plomb basées sur l'alliage inorganique $CsSnGeI_3$. Il présente les fondements du photovoltaïque, les propriétés des matériaux pérovskites et l'optimisation de la cellule par simulation sous SCAPS-1D. L'étude met en évidence qu'une épaisseur d'absorbeur de 1000 nm et l'association $CuSbS_2$/ZnO donnent les meilleures performances, avec un rendement simulé d'environ 22,83 %. Elle montre également que la température et les défauts du matériau influencent fortement la stabilité et l'efficacité du dispositif.

Mots-Clés : Cellules solaires en pérovskite sans plomb, CsSnGeI 3, simulation SCAPS-1D, optimisation des cellules solaires.

ملخص

تتناول هذه المذكرة خلايا شمسية بيروفسكايت خالية من الرصاص تعتمد على السبيكة غير العضوية ($CsSnGeI_3$).وتعرض أساسيات التحويل الكهروضوئي وخصائص مواد البيروفسكايت، ثم تستخدم محاكاة SCAPS-1D من أجل تحسين أداء الخلية. وقد بينت الدراسة أن سماكة طبقة الامتصاص المثلى هي 1000 نانومتر، وأن الجمع بين $CuSbS_2$ وZnO في طبقات النقل يعطي أفضل النتائج مع كفاءة محاكاة تقارب 22.83٪ كما أوضحت أن ارتفاع درجة الحرارة ووجود العيوب في المادة يؤثران بشكل كبير في استقرار الخلية وأدائها.

الكلمات المفتاحية: الخلايا الشمسية البيروفسكايتية الخالية من الرصاص، $CsSnGeI_3$، محاكاة SCAPS-1D، تحسين الخلايا الشمسية.

Summary:

Remerciements: ..... **I**

Summary: ..... **III**

list of Figures: ..... **V**

list of Tables: ..... **VIII**

Abbreviation: ..... **IX**

General Introduction **1**

Bibliography for General Introduction 3

Chapter I: Fundamentals of Photovoltaic Solar Cells **4**

I.1. Introduction 5

I.2.General Overview of Solar Energy 5

I.2.1.the spectrum of the sun 5

I.2.2. Solar radiation 7

I.2.3 Solar Energy Conversion 8

I.3 Photovoltaic Cell Fundamentals 9

I.3.1 History 10

I.3.2 Physical Structure 10

I.3.3 Working Principle 11

I.3.4 Performance Parameters 12

I.4 Modelling and Characteristics of PV Cells 13

I.4.1 Electrical Model 13

I.4.2 Electrical Characteristics 15

I.5 Different Generations of Solar Cell 17

I.5.1 First-Generation Solar Cell 18

I.5.2 Second-Generation Solar Cells 20

I.5.3 Third-Generation Solar Cells 22

I.6 Conclusion 25

Bibliography for Chapter I 26

Chapter II: Perovskite Solar Cells **29**

II.1 Introduction 30

II.2 Fundamentals of Perovskite Materials 30

II.2.1 Definition of Perovskite Materials 30

II.2.2 Crystal Structure of Perovskites 30

II.2.3 Structural Properties of Perovskites 31

II.3 Perovskite Solar Cells 33

II.3.1 Operating Principle 33

II.3.2 Device Architecture 34

II.3.3 Charge Transport Mécanisme 36
II.4 Physical and Electronic Properties of Perovskite Materials 36
II.4.1 Band Gap Energy 37
II.4.2 Absorption Coefficient 37
II.4.3 Carrier Mobility 37
II.5 Classification of Perovskite Materials 38
II.5.1 Organic–Inorganic Perovskites 38
II.5.2 Inorganic Perovskites 38
II.5.3 Lead-Free Materials 40
II.6 Lead-Free Perovskite Absorber Material: $CsSnGeI_3$ 42
II.6.1 Chemical Composition of $CsSnGeI_3$ 42
II.6.2 Structural Properties 43
II.6.3 Optical Properties 43
II.6.4 Electrical Properties 44
II.6.5 Stability of $CsSnGeI_3$ 44
II.6.6 Advantages and Disadvantages and Challenges of $CsSnGeI_3$ 45
II.7 Applications and Future Prospects of Perovskite Solar Cells 46
II.7.1 Current Applications 46
II.7.2 Future Developments and Research Trends 47
II.8 Conclusion 48
Bibliography for Chapter II 49
Chapter III: Results and Discussion of the C_SSnGeI_3 Perovskite Solar Cell Simulation .. 53
III.1 Introduction 54
III.2 Presentation of the SCAPS-1D Software 54
III.3 Results and Discussion 58
III.3.1 The Structure Studied 58
III.3.2 Effect of the C_SSnGeI_3 layer thickness on the photovoltaic parameters of the solar cell 60
III.3.3 Simulation of a perovskite solar cell using different HTL layer materials 63
III.3.4 Simulation of a perovskite solar cell using different ETL layer materials 65
III.3.5 Effect of temperature on the photovoltaics parameters solar cell 68
III.4 Conclusion 71
Bibliography for Chapter III 72
General conclusion: 74

list of Figures:

Chapter I: Fundamentals of Photovoltaic Solar Cells

Figure (I.1): The extra-terrestrial solar spectrum (AM = 0), the theoretical black body curve and the solar spectrum at the earth's surface for AM = 2 and the absorbed regions shown in black . 6
Figure (I.2): Spectral Distribution of Solar Radiation 7
Figure (I.3): Representation of Solar radiation components 8
Figure (I.4): Diagrammatic illustration of how solar radiation is converted into energy using a photovoltaic solar panel 9
Figure (I.5): a) Three-dimensional (3D) view of a conventional solar cell featuring front and back contacts. b) Two-dimensional (2D) cross-section of a conventional solar cell. 11
Figure (I.6): The structure of p-n junction and flow mechanism of PV cell 12
Figure (I.7):Formation of Depletion Zone. It is adapted from reference 12
Figure (I.8): real circuit Equivalent electrical diagram of the PV cell with a diode 13
Figure (I.9) : Circuit équivalent d'une cellule photovoltaïque idéale 14
Figure (I.10): I – V and P – V characteristics of a typical solar cell 16
Figure (I.11): Different kinds of solar cells and recent developments 18
Figure (I.12): Manufacturing chain of photovoltaic modules 19
Figure (I.13): Monocrystalline silicon wafer. 19
Figure (I.14): Polycrystalline silicon wafer. 20
Figure (I.15): Structure of CdTe cell: (a) substrate configuration; (b) superstrate configuration 21
Figure (I.16): Basic structure of typical CIGS solar cell 22
Figure (I.17): Dye sensitized solar cell DSSC diagram 23
Figure (I.18): Typical structure of a perovskite solar cell 23
Figure (I.19): OPV's operating principles 24

Chapter II: Perovskite Solar Cells

Figure (II.1): Generic ABX_3 metal-halide perovskite framework and octahedral connectivity 31
Figure (II.2): the main structural elements that affect halide perovskites' characteristics 32
Figure (II.3): The methods for producing artificial templates and halide perovskite..... 33
Figure (II.4): Band diagram and operating principle of a perovskite solar cell 34
Figure (II.5): A chronology of the evolution of perovskite solar cells from conventional to novel designs 35
Figure (II.6): An example of literature values for the energy levels in relation to the vacuum level of several materials that function as hole-selective layers (right), electron-selective layers

(left), and perovskite absorbers in perovskite solar cel 36
Figure (II.7): Illustration of the perovskite structure based on corner sharing octahedra of BX6 with either a monovalent metal (inorganic) or charged molecule (hybrid) at the centre of the unit cell. 39
Figure (II.8): Scheme for Inorganic Perovskites for Energy Applications 39
Figure (II.9): Schematic illustration of conventional 3D perovskites and four representative lead-free perovskites or perovskite derivatives with different dimensions in structure and morphology levels 40
Figure (II.9): Candidate elements for lead replacement in perovskite-type compounds 41
Figure (II.10): Schematic Illustration of Efficiency and Stability Enhancement Strategies in Lead-Free Perovskite Solar Cells 42
Figure (II.11): The crystal structure of CsSnGeI3 43
Figure (II.12): The figure outlines the development of halide perovskite materials-based applications 46

Chapter III: Results and Discussion of the C_SSnGeI_3 Perovskite Solar Cell Simulation

Figure III.1: The action or main window for the SCAPS startup..... 55
Figure III.2: Solar cell structure definition. 56
Figure III.3: Characteristics of a CsSnGeI3 Perovskite cell layer..... 57
Figure III.4: Display panel for the I-V curves 58
Figure III. 5: a) $CsSnGeI_3$-based PSC structure and b) charge carrier movement 59
Figure III.6 Effect of the thickness of the CSSnGeI3 absorber layer on the I-V characteristics of the solar cell 61
Figure III.7: Effect of the thickness of the CSSnGeI3 absorber layer on the EQE characteristics of the solar cell 62
Figure III.8: Effect of the thickness of the CSSnGeI3 layer on the photovoltaic parameters of the solar cell..... 62
Figure III.9 Influence of different HTL layer materials on the I-V characteristics of the solar cell 64
Figure III.10 Influence of different HTL layer materials on the EQE characteristics of the solar cell 65
Figure III.11 Influence of different ETL layer materials on the I-V characteristics of the solar cell 67
Figure II.12 Influence of different ETL layer materials on the EQE characteristic of the solar cell 68

Figure III.13 Effect of temperature on the I-V characteristics of solar cell 69
Figure III.14 Effect of temperature on the photovoltaïques parameters solar cell 70

list of Tables:

Chapter I: Fundamentals of Photovoltaic Solar Cells

Table (I.1): Subdivision of Ultra violate radiation 6
Table (I.2): Distribution of extra-terrestrial solar radiation 6

Chapter III: Results and Discussion of the $CsSnGeI_3$ Perovskite Solar Cell Simulation

Table (III.1) Device parameters such as FTO, HTL, ETL, and the CSSnGeI3 absorber layer are used for PSCs configuration 60
Table (III.2). Results showing the effect of the thickness of the CSSnGeI3 absorber layer on the photovoltaic parameters of the solar cell 61
Table (III.3) Physical properties of the various materials used in the HTL layer.....63
Table (III.4). Effects of different HTL layer materials on the photovoltaic performance of perovskite solar cells. 64
Table (III.5): Physical Parameters of the Different Materials of the ETL Layer.....66
Table (III.6). Results of the perovskite solar cell with different ETL layer materials on 67
Table (III.7). Results of the effects of temperature variations (300–450 K) on the photovoltaic parameters of a perovskite solar cell.....69

Abbreviation:

ABX_3	General formula of a perovskite
AM	Air Mass
AM0 / AM1.5G	Standardized solar spectra
BIPV	Building-Integrated Photovoltaics
c	Speed of light
CB	Conduction Band
CBTS	Copper Barium Tin Sulfide
CdTe	Cadmium Telluride
CFTS	Copper Iron Tin Sulfide
CIGS	Copper Indium Gallium Selenide
$CsSnGeI_3$	Cesium Tin Germanium Iodide
CZ	Czochralski (crystal growth method)
DSSC	Dye-Sensitized Solar Cell
Eg	Band gap (forbidden band)
EQE / QE	External Quantum Efficiency / Quantum Efficiency
ETL / ETM	Electron Transport Layer / Material
eV	Electron-volt
FF	Fill Factor
FTO	Fluorine-doped Tin Oxide
h	Planck's constant
HTL / HTM	Hole Transport Layer / Material
I	Current
I_0 / Isat	Saturation current
Iph	Photocurrent
Isc / Jsc	Short-circuit current / Short-circuit current density
Jn / Jp	Electron / hole current density
k	Boltzmann's constant
MA / FA	Methylammonium / Formamidinium
n	Ideality factor
NA	Acceptor doping concentration
NC / NV	Effective density of states in the conduction / valence band
ND	Donor doping concentration
nm / µm	Nanometer / micrometer
Nt	Defect density
OPV	Organic Photovoltaics
PCE	Power Conversion Efficiency
Pin / Pinc	Incident power
Pmax	Maximum power
PSC	Perovskite Solar Cell
PV	Photovoltaic
q	Elementary charge
R	Recombination rate

rA, rB, rX	Ionic radii of sites A, B and X
Rs	Series resistance
Rsh / Rp	Shunt / parallel resistance
SCAPS-1D	Solar Cell Capacitance Simulator 1D
SRH	Shockley–Read–Hall (recombination)
STO	Strontium Titanate
t	Goldschmidt tolerance factor
T	Temperature
V	Voltage
VB	Valence Band
Voc	Open-circuit voltage
VT	Thermal voltage
ZnO	Zinc Oxide
εr	Relative permittivity
η	Conversion efficiency
λ	Wavelength
μ	Octahedral factor
μn / μp	Electron / hole mobility
ν	Frequency
χ	Electron affinity
Ψ	Electric potential
ABX_3	General formula of a perovskite
AM	Air Mass
AM0 / AM1.5G	Standardized solar spectra

General Introduction

The growing global demand for clean, reliable, and sustainable energy has intensified interest in photovoltaic technologies as a strategic response to climate change, fossil fuel depletion, and the need for low-carbon electricity generation. Among the available renewable resources, solar energy occupies a central position because of its abundance, wide geographical availability, and direct conversion potential through semiconductor devices. Over the past decades, photovoltaic solar cells have evolved from a niche technology primarily used in space applications to a major component of modern energy systems. Nevertheless, the continued improvement of solar cell performance, cost-effectiveness, material sustainability, and long-term stability remains a major scientific and technological challenge. Recent reviews have underlined that the future of photovoltaics depends not only on efficiency gains but also on advances in materials engineering, scalable fabrication, and environmental compatibility [1–5].

Within this broader context, perovskite solar cells have emerged as one of the most promising third-generation photovoltaic technologies. Their remarkable optoelectronic properties, tunable bandgap, strong light absorption, and compatibility with relatively low-temperature processing have positioned them at the forefront of current solar cell research. At the same time, important limitations still hinder their large-scale deployment, particularly issues related to operational stability, defect sensitivity, and the environmental concerns associated with lead-containing perovskite absorbers. As a result, the search for lead-free perovskite materials has become an important direction in the development of sustainable photovoltaic devices. In this regard, tin- and germanium-based compounds have attracted growing attention as potentially fewer toxic alternatives capable of preserving favorable electronic and optical properties while reducing environmental risk [2][3][4][5].

This thesis is situated within that scientific effort and focuses on the study of photovoltaic solar cells with particular emphasis on lead-free perovskite materials. The work aims to establish a coherent progression from the fundamental principles of solar energy conversion to the materials science of perovskite absorbers and finally to the numerical optimization of a lead-free perovskite solar cell structure. Special attention is given to the inorganic alloy CsSnGeI3, which represents a promising candidate for next-generation photovoltaic applications owing to its suitable bandgap, high absorption coefficient, and potential for improved chemical stability compared with purely tin-based systems.

The first chapter presents the fundamentals of photovoltaic solar cells. It introduces the nature of solar radiation, the photovoltaic effect, and the physical principles governing solar energy conversion. It also reviews the main generations of solar cells and discusses the key electrical parameters used to evaluate device performance, such as open-circuit voltage, short-circuit current, fill factor, and power conversion efficiency. This theoretical foundation is essential for understanding the behavior of photovoltaic devices and for interpreting the performance of advanced solar cell structures.

The second chapter focuses on perovskite solar cells, with particular emphasis on their crystal structure, operating mechanism, and classification. It highlights the rapid development of this technology and examines the transition from conventional lead-based perovskites toward environmentally safer alternatives. In this framework, the chapter discusses the structural, optical, and electronic characteristics of CsSnGeI3, emphasizing its relevance as a lead-free absorber material and its potential role in reconciling device performance with sustainability considerations.

The third chapter is devoted to the numerical simulation and optimization of a lead-free perovskite solar cell based on CsSnGeI3 using the SCAPS-1D simulation tool. The study investigates the influence of absorber thickness, charge transport layers, and operating temperature on the photovoltaic performance of the device. Through this approach, the thesis seeks to identify an optimized cell architecture and to assess the theoretical potential of this material system for high-efficiency and environmentally responsible solar energy conversion. Overall, this thesis aims to contribute to ongoing research on sustainable photovoltaics by combining fundamental analysis, material-oriented investigation, and simulation-based optimization. By exploring the performance of a lead-free perovskite absorber within a structured theoretical and numerical framework, the work intends to support the development of safer and more efficient photovoltaic technologies for future energy applications.

Finally, we draw a general conclusion and Future outlook**.**

Bibliography for Introduction general

[1] Afre, R. A., & Pugliese, D. (2024). Recent Advances in Materials, Fabrication Techniques, and Stability Enhancement Strategies for Perovskite Solar Cells. Micromachines, 15(2), 192.

[2] Khan, A. D., Mustajab, M., Moeen, S., Imran, M., Ikram, M., Khan, Q., & Khan, M. (2024). Advancements in the stability, protection and lead-free strategies of perovskite solar cells: a critical review. Environmental Science: Advances, 3, 1004-1029.

[3] Zhou, Q., Liu, X., Liu, Z., Zhu, Y., Lu, J., Chen, Z., Li, C., Wang, J., Zhang, H., & Chen, W. (2024). Annual research review of perovskite solar cells in 2023. Materials Futures.

[4] Miah, M. H., Khandaker, M. U., Hossen, M. J., et al. (2025). Lead-free alternatives and toxicity mitigation strategies for sustainable perovskite solar cells: a critical review. Materials Advances, 6, 2718-2752.

[5] Araujo, V. H. D., Nogueira, A. F., Tristao, J. C., & dos Santos, L. J. (2025). Advances in lead-free perovskite solar cell design via SCAPS-1D simulations. RSC Sustainability, 3, 4314-4335.

Chapter I: Fundamentals of Photovoltaic Solar Cells

I.1. Introduction

By permitting the direct conversion of sunlight into electricity using electronic materials, solar cell technology has experienced substantial evolution and represents a crucial feature of the energy shift. Solar cells, which were first created to power space missions, are now crucial parts of terrestrial energy systems. The materials used to make solar cells are important because they affect how well the cells work with electricity, like how voltage they make. This chapter reviews some fundamental ideas on the photovoltaic effect, the principle of the solar cell, and the load in order to help readers better grasp this Phenomena.

I.2.General Overview of Solar Energy

In recent years, solar energy has attracted significant attention because it accounts for the majority of renewable energy sources. Solar energy strikes the Earth's surface at a rate of 120 petawatts (1 petawatt = 10^{15} w). This means that all the solar energy received from the sun in a single day could meet the entire world's demand for several decades [1].

I.2.1.the spectrum of the sun

Solar spectrum is the distribution of the sun's energy by wavelength, that is, how sunlight is separated into distinct categories (ultraviolet rays, visible light, and infrared rays). With wavelengths ranging from roughly 0.2 μm to 2.6 μm, the sun's radiation provides a fair approximation of black body radiation, which is a continuous distribution of wavelengths with no wavelengths missing (Fig. I.1)[2] .

The solar spectrum consists of:

- ultraviolet radiation in the range of 200 to 400 nm.
- visible light in the range of 390 nm (violet) to 740 nm (red).
- infrared radiation in the range of 700 nm 1 mm.

Table (I.1) shows the subdivisions of the Ultra violate range and Table (I.2) shows the distribution of extra -terrestrial solar radiation.

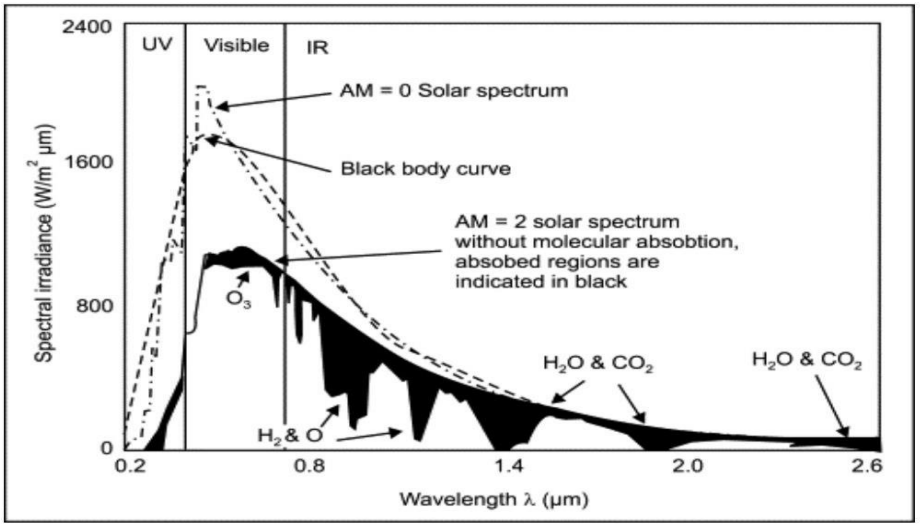


Figure (I.1): The extra-terrestrial solar spectrum (AM = 0), the theoretical black body curve and the solar spectrum at the earth's surface for AM = 2 and the absorbed regions shown in black [3].

Table (I.1): Subdivision of Ultra violate radiation [3].

Wavelength Range (nm)	Effect
320 – 400 nm	Not harmful in normal doses, vitamin D production
290 – 320 nm	Tanning, can burn
230 – 290 nm	Causes skin cancer

Table (I.2): Distribution of extra-terrestrial solar radiation [3].

Radiation Type	Wavelength Range (nm)	Percentage (%)
Ultra violet	200 - 400	8.7 %
Visible	400 -700	38.3 %
Near Infrared	700 -3500	51.7 %

As sunlight passes through the atmosphere, certain wavelengths get absorbed, and some of the total energy gets scattered. That's why the solar spectrum reaching Earth's surface has gaps in those wavelengths (the dark parts in Fig. (I.1)) and overall lower intensity.

I.2.2. Solar radiation

The Sun is a massive gaseous orb that emits substantial energy through the fusion of hydrogen nuclei, manifested as solar radiation. Sun is producing roughly 6.4*107 W/m2. Out of which ~ 1370 W/m2 is incident on the Earth's atmosphere supposing no absorption of sunlight in space and roughly 980 W/m2 power density reaches Earth's surface [3].

Electromagnetic radiation released by the Sun encompasses a wide variety of wavelengths, providing a continuous spectrum [4]. Figure (I.2) illustrates the spectral distribution of solar radiation across different wavelengths, highlighting how the intensity of the radiation varies across the spectrum.

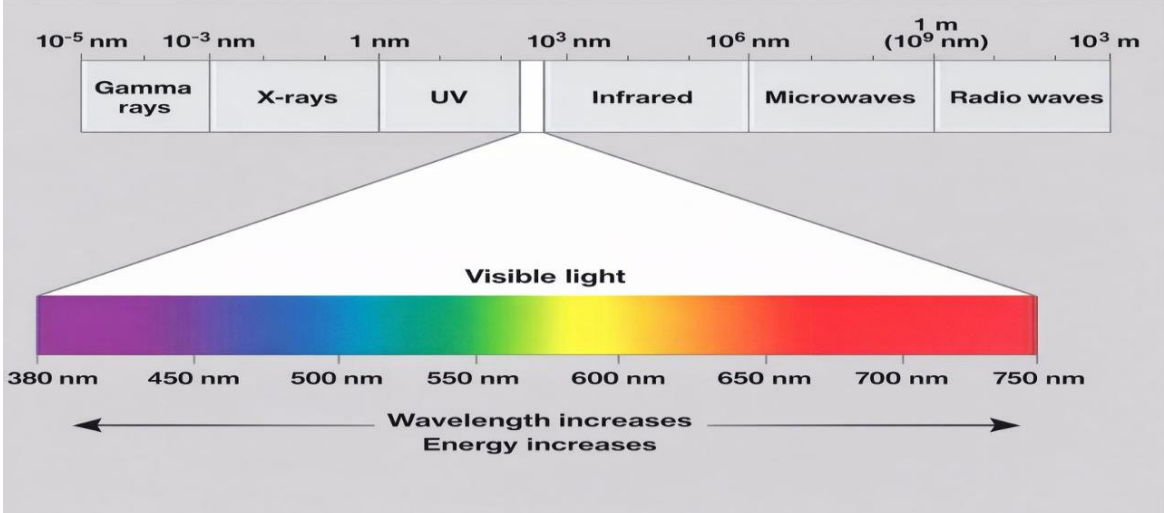


Figure (I.2): Spectral Distribution of Solar Radiation[5].

Direct radiation and diffuse radiation are two main types of solar radiation reaching the Earth's surface. Direct radiation is the solar energy hitting the Earth's surface directly from the Sun, free from atmospheric scattering or interference. Conversely, diffuse radiation is solar energy reaching the Earth's surface following dispersion during its passage through the atmosphere. The strength of this radiation depends on elements including pressure of light beams, altitude, and angle of impact. Essential components of solar radiation are shown in Figure (I.3), emphasizing reflected radiation, diffuse radiation, and direct radiation[6] .

The power supplied by the radiation, is obtained by integrating the irradiance throughout the whole spectrum. The following ideas are utilized for simplicity[7] :

- AM0: Outside the atmosphere (space applications). P = 1.36 kW.m^{-2}
- AM1: The sun is at the zenith of the observation location (at the equator).
- AM1.5G: Standard spectrum, the sun is at 45°. P = 1KW. m^{-2}

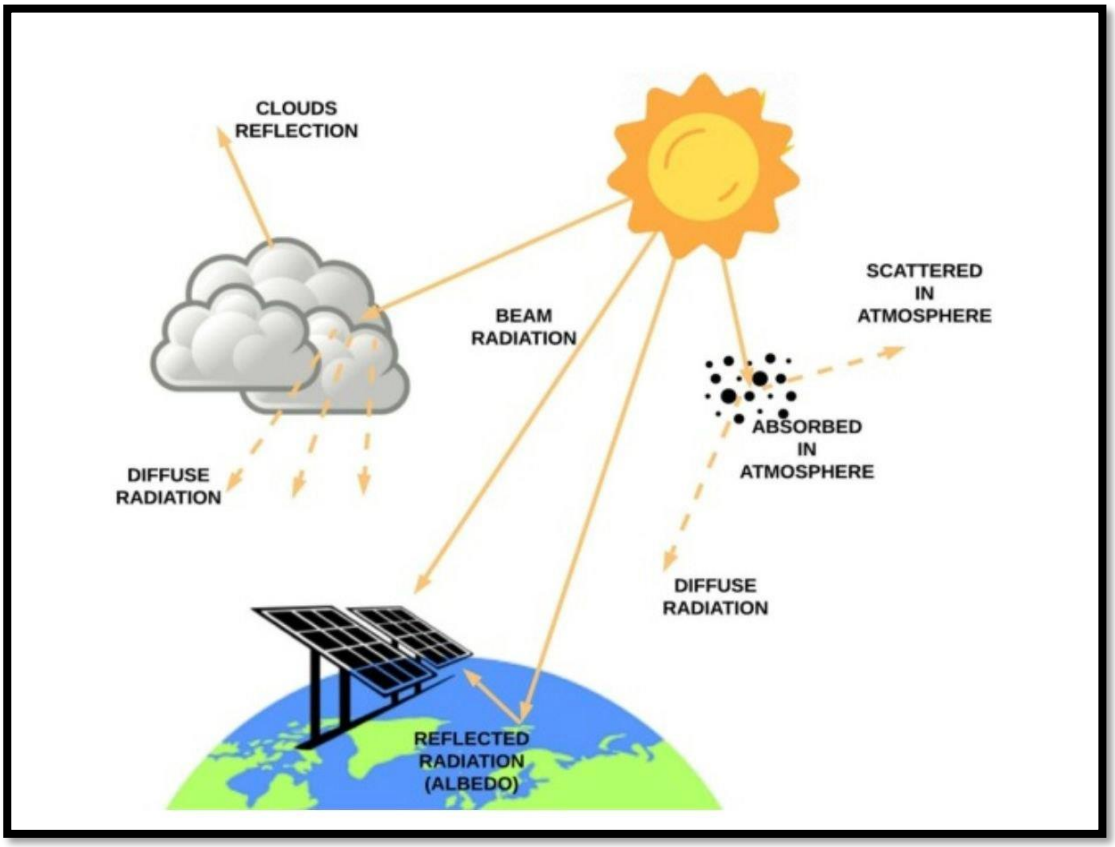


Figure (I.3): Representation of Solar radiation components [8].

I.2.3 Solar Energy Conversion

Solar energy is the result of the Sun's energy being transformed into thermal and electrical energy. One of the most plentiful sources of renewable energy is this. Photovoltaic solar cells transform the thermal and light energy emitted by the Sun into electrical and thermal energy (Fig. 4). Along with wind power, it is one of the low-carbon energy technologies. Since the goal is to surpass the demand for clean energy and lessen the world's reliance on fossil fuels, developing sustainable energy supplies is a difficult endeavour for humans. Solar energy is one of the most promising, long-lasting, universal, large-capacity, and ecologically acceptable forms of renewable and sustainable energy. Although natural sun irradiation is dispersed and discontinuous, the actual usage of solar energy utilizing modern and clean technology remains a big problem [9].

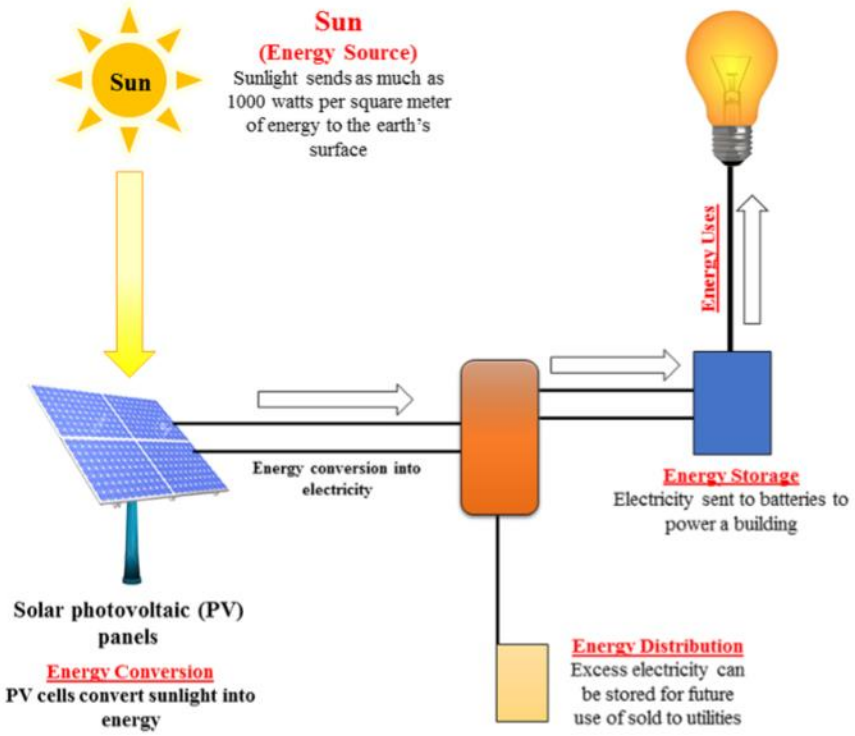


Figure (I.4): Diagrammatic illustration of how solar radiation is converted into energy using a photovoltaic solar panel [36].

Albert Einstein discovered that light was more than just a wave and that its energy was transmitted by photons, which are particles, while studying the photoelectric phenomenon. The energy of a photon is provided via the following connection:

$$E = h.\nu = \frac{h\,c}{\lambda} \qquad (I.1)$$

E: Energy in electron volts (eV).

h: Planck's constant (6.626×10^{-34}(j. s −1)).

C: the speed of light (3×10^{8}(m/s)).

λ: the wavelength (m).

ν: frequency (s-1).

I.3 Photovoltaic Cell Fundamentals

At their core, photovoltaic cells stand out as sophisticated devices that harness semiconductor properties to act as a vital medium, they capture the energy of light photons and convert it directly into electrical current through the photovoltaic effect. The engineering of these cells is embodied in the p-n junction typically crafted from silicon which serves as the functional heart responsible for sensing light and generating power the moment rays strike its

surface, this junction generates "electron-hole" pairs. These charge carriers are separated by the internal electric field present at the junction and subsequently collected at the exterior contacts, resulting in a photocurrent and photovoltage.

The following sections review the historical development of this technology and examine in detail the underlying physics upon which it is based.

I.3.1 History

The history of photovoltaic cells spans over two centuries, dating back to 1839 when French scientist Edmond Becquerel first characterised the photovoltaic effect while conducting electrochemical experiments, he observed this action on silver and platinum electrodes exposed to sunshine. The first selenium-based solar cell was invented in 1876 by scientist Adams and his student Richard, with an efficiency of 0.5%. a year later, physicist Charles Fritsch succeeded to double this efficiency using selenium but by a different way [9].

In 1958, photovoltaic technology was first used in space satellites. Since solar cells became the main energy source for spacecraft, governments have invested in this technology, which has seen notable improvements in efficiency, especially in cells based on monocrystalline silicon, whose efficiency reached 22% to 24% in 1980, and which are still used to produce energy today[10] .

I.3.2 Physical Structure

The physical structure of a standard crystalline silicon solar cell has been developed throughout decades of study and manufacturing optimisation. A standard industrial silicon solar cell is a planar structure including several unique functional layers, each fulfilling a specific purpose in the photon absorption and carrier collecting process.

A photovoltaic solar cell is made of three main parts:

- Light Absorber: converting incident photons to electron and holes.
- Carrier Collector: capturing the carriers - electrons and holes.
- Metal Contacts: transferring the carriers to the circuit (Ag, Au).

A conventional solar cell structure is simply based on a semiconductor p-n junction diode that operates under solar illumination as sketched in figure (I.5), by breaking the quasi-particle's exciton link the semiconductor substance that makes up the cell absorbs light energy and converts it straight into electric current.

The main physical component of the cell is typically a p-type silicon wafer, 160 to 200 **µm** thick, doped with boron. The emitter is a p-type surface layer, approximately 0.3 **µm** thick, consisting of phosphorus deposited on the front surface of the silicon wafer. As for the other

layer, which serves as the anti-reflective coating, it is typically made of silicon nitride (Si_3N_4). It plays a role in reducing light reflection losses, which leads to increased photon absorption and improved efficiency[11] .

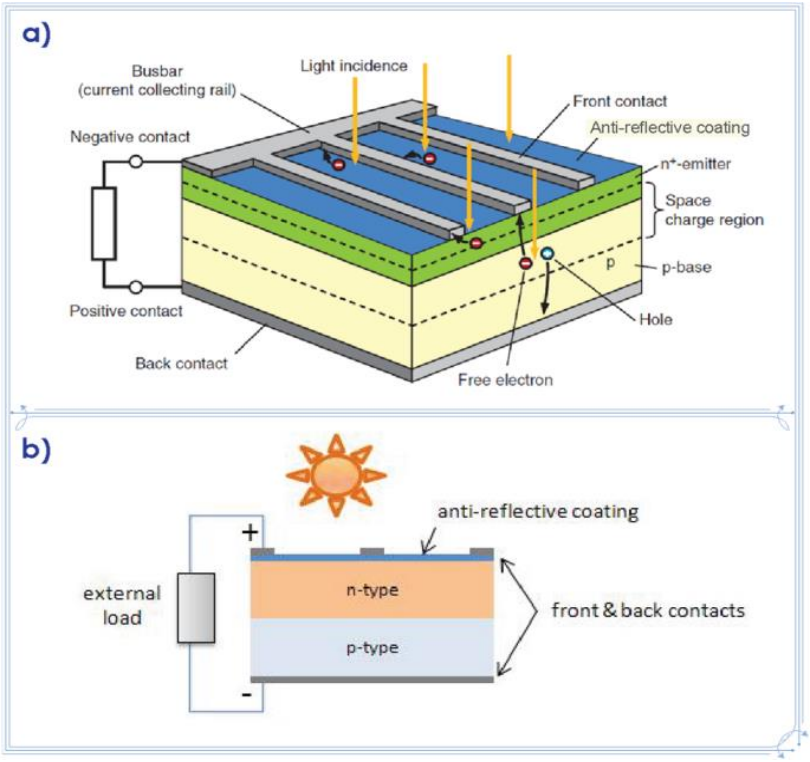


Figure (I.5): a) Three-dimensional (3D) view of a conventional solar cell featuring front and back contacts. b) Two-dimensional (2D) cross-section of a conventional solar cell[10] .

I.3.3 Working Principle

Solar energy is turned into electrical energy within the framework of the photovoltaic effect. When a PV cell is exposed to solar energy, as much photon energy as absorbed is transformed. The PV cell comprises numerous atoms and electrons are stimulated by the absorbed energy and produce electrical flow by leaving their places. Thanks to the electrical flow, energy is released and with this energy, by employing an external electrical circuit, the PV cell makes an electric current. In order to form the electrical field, two separate semiconductor layers, n-type and p-type, are present in the PV cell in contact with each other. The first layer that is n-region is negatively charged while the second layer, the p-region, contains positively charged ions [12]. There are negative and positive charges inside the PV cell due to the atoms. Since n-type includes more electrons and p-type contains more holes, p-n junction arises between the contacting interfaces. Both the passage of positive and negative

ions contributes to the creation of the electric field. Electrons depart from the semiconductor surface and travel to the negative surface to transport current due to the generated electric field. To make room for the incident electrons, the holes simultaneously travel to the positive surface in the opposite direction of the electron migration. Figure (I.6), shows a schematic representation of current flow and p-n junction development in a solar cell.

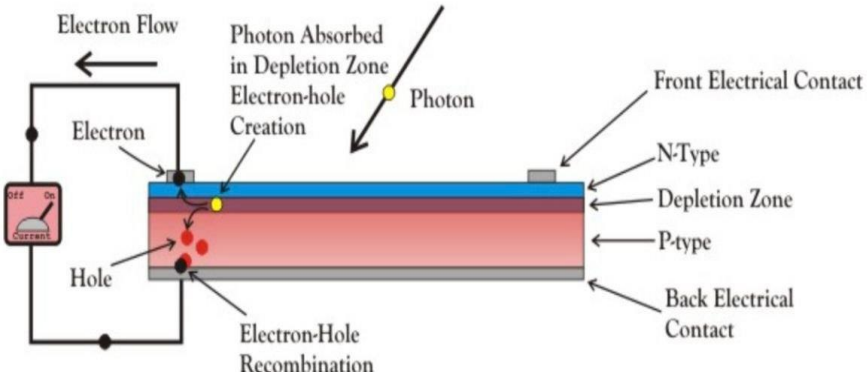


Figure (I.6): The structure of p-n junction and flow mechanism of PV cell [12].

A particular area between the n-type and p-type contact regions is depicted in figure (I.7). In this area, the force acting on holes travelling in the n-region is equal to that acting on electrons moving in the p-region. Like the gaps in the n-region, these electrons are thus locked inside the p-region. This force creates what is known as a depletion zone between the two layers. Electric current is generated in the p-n junction's depletion zone [13].

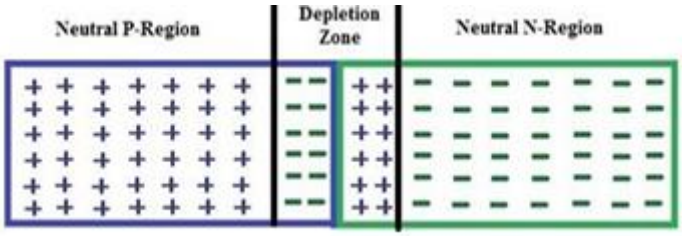


Figure (I.7): Formation of Depletion Zone. It is adapted from reference [12].

I.3.4 Performance Parameters

The quality of a photovoltaic cell lies in its performance and its ability to convert the solar spectrum into exploitable electrical energy. It is an essential part in evaluating the efficiency of solar systems.

One of the most striking aspects of performance is the amount of electrical energy that a cell can produce under standard conditions. The higher the electrical power, the better the performance. Moreover, the quality of materials and manufacturing technology of the cell play

an important role in determining the overall performance. As the higher the quality of the material helps to reduce energy losses and increase efficiency.

Improving cell performance is a key goal in sustainable energy research, as it allows the production of alternative energy with great efficiency.

I.4 Modelling and Characteristics of PV Cells

I.4.1 Electrical Model

I.4.1.1 Real Model

Photovoltaic cells can be represented by an equivalent electrical circuit that elucidates their behaviour under solar radiation exposure. This model is widely used to analyse and evaluate the performance of solar cells.

This equivalent circuit consists of a current source (Iph) representing photons, a diode representing the PN junction, a series resistance (Rs) representing losses due to the Joule effect, and a shunt resistance (Rsh) representing the leakage current. This is illustrated in the figure (I.8) [14], [15].

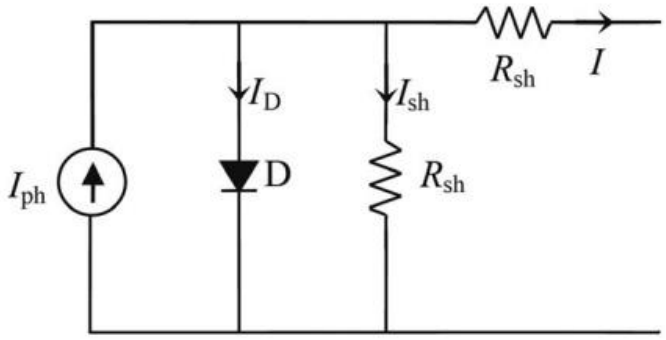


Figure (I.8): real circuit Equivalent electrical diagram of the PV cell with a diode [14].

Kirchhoff's law allows us to write the following relationship:

$$I_{ph} = I_D + I_p + I \longrightarrow I = I_{ph} - I_D - I_{sh} \qquad (I.2)$$

The current passing through a load is expressed as:

$$I = I_{ph} - I_0 \left[\exp\left(\frac{V+I.R_s}{V_T}\right)-1\right] - \frac{V.I.R_s}{R_{sh}} \qquad (I.3)$$

I_{ph}: Photocurrent generated by the cell (proportional to the incident irradiance).

I: Current generated by the photovoltaic cell.

I_0: Reverse saturation current of the diode.

V: Output voltage.

R_{sh}: Shunt resistance representing leakage currents around the p–n junction due to impurities and at the cell edges.

R_s: Series resistance representing the bulk resistance of the semiconductor material, as well as the ohmic and contact resistances at the cell connections.

I.4.1.2 Ideal Model

A current source connected in parallel to a single diode is the perfect analogue circuit for a photovoltaic cell. Figure (I.9), depicts the setup of the single-diode simulated perfect solar cell [15].

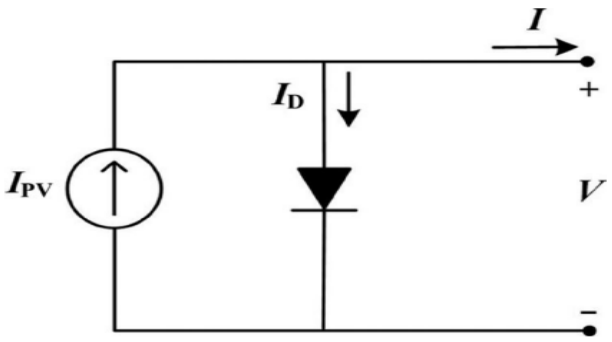


Figure (I.9) : Circuit équivalent d'une cellule photovoltaïque idéale [14].

In this context, the current–voltage (I–V) curve of the equivalent circuit is expressed using equation, following[16].

$$I = I_{pv} - I_d \qquad (I.4)$$

I: is the current delivered by the cell.

I_{pv}: is the photocurrent of the cell, proportional to the irradiance.

$$I_d = I_0[\exp(\frac{V}{\alpha V_T})\text{-}1] \quad \text{and} \quad V_T = \frac{kT}{q} \qquad (I.5)$$

Consequently, the present equation provided by the photovoltaic solar cell is as follows:

$$I = I_{pv} - I_0 \left[\exp\left(\frac{V}{\alpha V_T}\right) - 1\right] \quad (I.6)$$

I_0 : Reverse saturation current of the diode.

V_T: Thermal voltage.

k: Boltzmann constant (1.38×10^{-23} J/Kelvin).

T: Cell temperature in Kelvin.

q: Electron charge (1.6×10^{-19} C).

α: Ideality factor of the junction.

V: Voltage across the cell.

I.4.2 Electrical Characteristics

Besides series and shunt resistance, the performance of photovoltaic solar cells is primarily defined by 5 critical parameters: (1) short-circuit current density, (2) open-circuit voltage, (3) maximum power output, (4) fill factor, and (5) solar energy to power conversion efficiency, which are elaborated upon below [17].

I.4.2.1 Short-Circuit Current (Isc)

The short-circuit current density, denoted as Isc, refers to the current flowing through a solar cell with an area of one square centimetre when the impedance is minimal and the voltage across the solar cell is zero. The Isc results from the creation and accumulation of charge carriers produced by light. In an optimal solar cell, under conditions of minimal resistive loss mechanisms, the short-circuit current density (Isc) and the light-generated current are equivalent. By removing the voltage V from equation (I.7), we obtain the following: Isc is essentially dependent on the area of the solar cell and the number of photons that reach the junction [17].

$$I_{sc} = I_{ph} - I_{sat}\left[\exp\left(\frac{q(I_{cc} * R_s)}{nkT}\right) - 1\right] - \frac{(I_{cc} * R_s)}{R_{sh}} \quad (I.7)$$

I.4.2.2 Open-Circuit Voltage (Voc)

The open circuit voltage (Voc) is the greatest voltage obtainable from a solar cell at zero current. The open circuit voltage reflects the cell's direct polarisation caused by light-generated current at the junction.

$$0 = I_{cc} - I_{sat}\left[\exp\left(\frac{q*V}{nKT}\right) - 1\right] - \frac{V}{R_{sh}} \quad \text{and} \quad V_{co} = V_t \ln\left[\frac{I_{ph}}{I_{sat}} + 1\right] \qquad (I.8)$$

I.4.2.3 Maximum power output

The power output of a solar cell is determined by multiplying the measured cell current by the bias voltage. The highest current and voltage that a solar cell can produce are Isc and Voc, respectively.

$$P_{max} = V_{oc} * I_{sc} \qquad (I.8)$$

The characteristic curve of a PV cell is really more "rounded" (Figure I.10), with the voltage at the maximum power point (Vp) being lower than the open-circuit voltage (Vp) and the supplied current (Vp) being lower than the short-circuit current (Vp) at the same voltage. At this point, the power can be stated as follows:

$$P_{max} = V_{pmax} * I_{pmax}$$

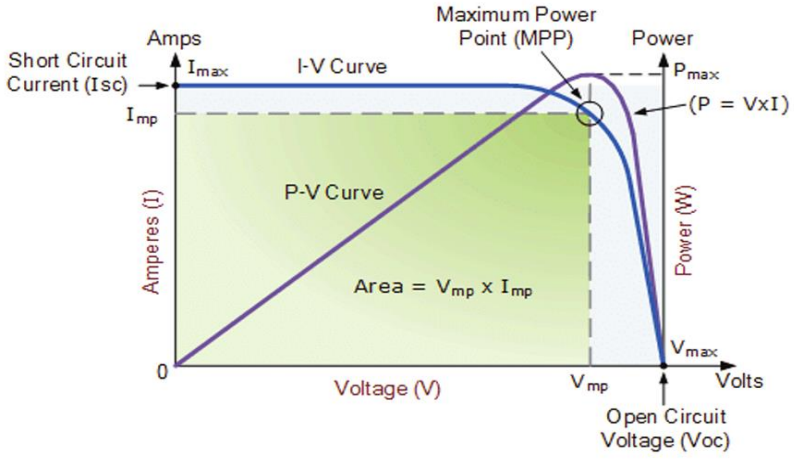


Figure (I.10): I – V and P – V characteristics of a typical solar cell [18].

I.4.2.4 Form factor

The fill factor (FF) is defined as the ratio of the maximum power output of the solar cell to the product of the open-circuit voltage (Voc) and the short-circuit current (Isc). Typically, the range of FF is from 0.50 to 0.82 or 50 to 82% as the FF is also represented in percentage using the following relation:

$$FF(\%) = \frac{I_m . V_m}{V_{oc} . I_{sc}} = \frac{P_m}{V_{oc} . I_{sc}} \quad (I.9)$$

I.4.2.5 Solar-to-electrical power conversion efficiency

The solar-to-electrical power conversion efficiency (η%) is a critical metric for evaluating the performance of a solar cell during testing. The η is defined as the ratio of energy production from the solar cell to the energy intake from the Sun. is dependent on the temperature of the solar cell as well as the spectrum and intensity of the incident sunlight. It also reflects the performance of the solar cell itself. It is commonly recognised that Isc, Voc, FF, and the incident light intensity (Pin) can be used to calculate an overall η (%) of the solar cells [17], [19]

$$\eta(\%) = \frac{FF . I_{sc} . V_{oc}}{P_{inc}} = \frac{P_{max\,out}}{P_{inc}} \quad (I.10)$$

I.5 Different Generations of Solar Cell

The growth of photovoltaic technology is typically divided into three (sometimes four) 'generations', each defined by the main materials, production approaches, efficiency levels, and cost structures. This generational paradigm, while somewhat simplified, provides a useful historical and technological narrative for understanding how the field has progressed and where it is heading[14], [20]. The three established generations are summarized in Figure (I.11) and discussed in detail below.

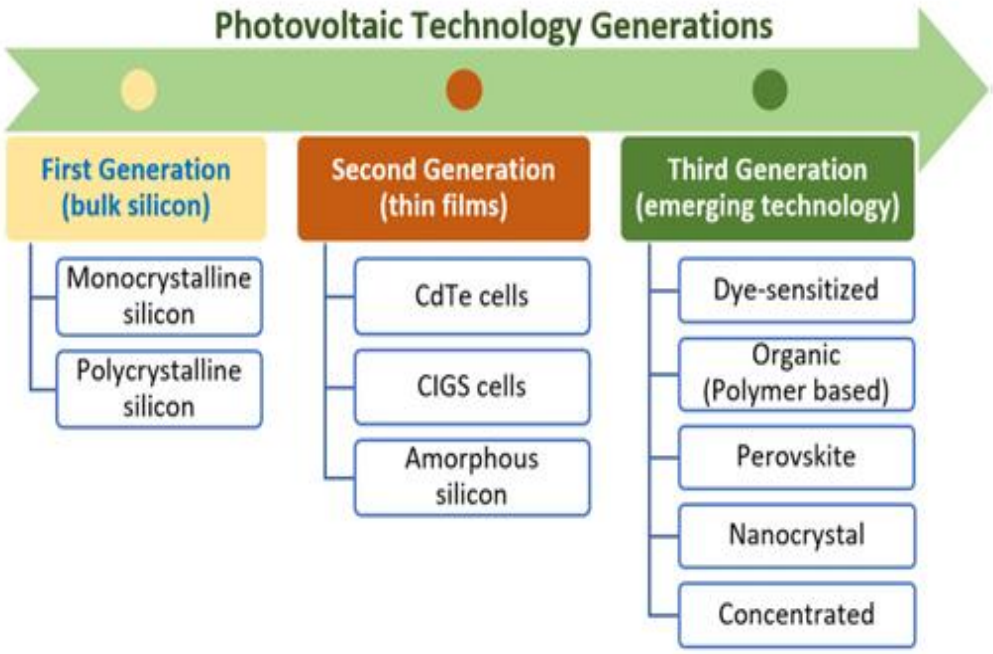


Figure (I.11): Different kinds of solar cells and recent developments[10].

I.5.1 First-Generation Solar Cell

These solar cells are made of crystalline silicon wafers. This technology uses the most expensive method for creating pure silicon crystal because it is made from crystalline silicon. These solar cells are employed in globally, and these are the most commercially efficient. Single crystalline solar cells account for about 80% of the solar cell market. According to Zhao et al. (1998), polycrystalline solar cells with a honeycomb-like structure have an efficiency of roughly 19.8% [21].

First-generation cells typically require less space for a given unit of electricity and are more effective at lower temperatures. Nevertheless, the primary drawback of these PV cells is that they perform worse at higher temperatures [22]. To manufacture silicon-based solar cells, several steps must be followed as shown in Figure (I.12).

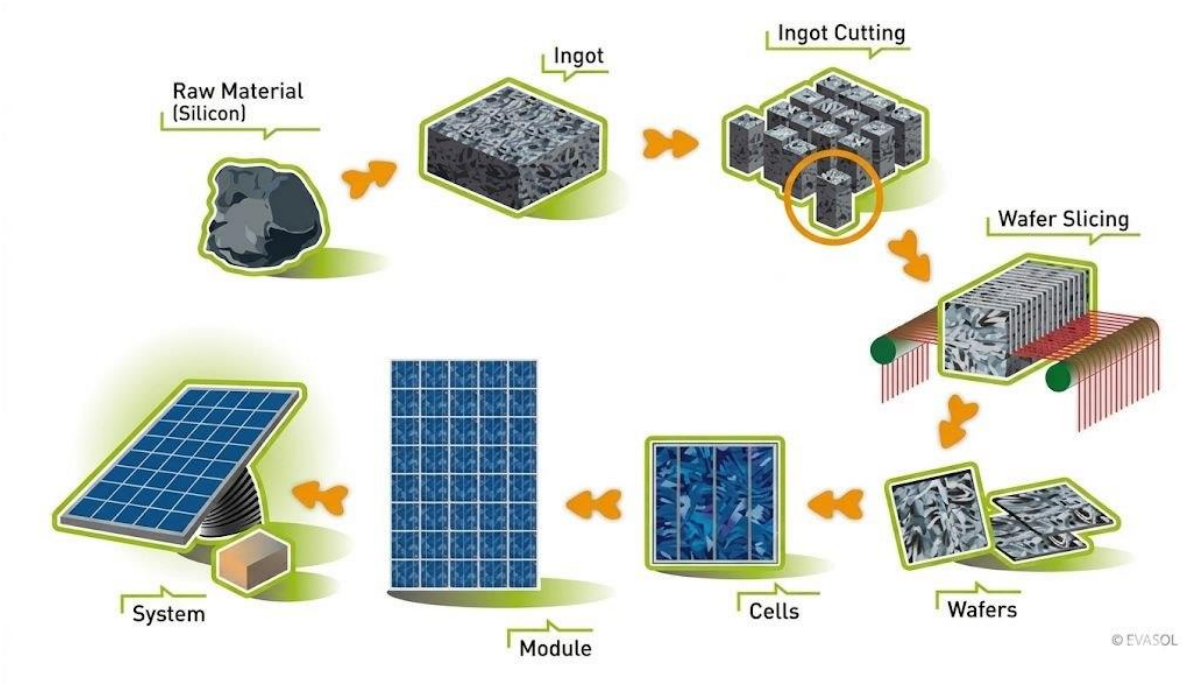


Figure (I.12): Manufacturing chain of photovoltaic modules [23] .

I.5.1.1 Monocrystalline Silicon (mono-Si)

Single-crystal silicon wafers cut from Czochralski (CZ) produced ingots are used to create monocrystalline silicon cells. High minority carrier lifetimes and diffusion lengths are produced by the regular crystal lattice devoid of grain boundaries, allowing for high efficiency[24]. To produce pure silicon, this method uses a lot of energy. The exceptional efficiency of monocrystalline cells (Figure I.13) ranges from 18% to 24%.

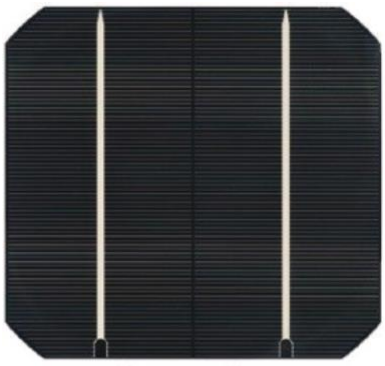


Figure (I.13): Monocrystalline silicon wafer.

I.5.1.2 Polycristalline Silicon (poly-Si or mc-Si)

Lower-cost cast silicon ingots with several crystal grains divided by grain boundaries are used to create polycrystalline (multi crystalline) silicon cells. Grain boundaries reduce carrier lifetimes and produce lower efficiency by acting as recombination centers. (17–20% commercial, 18–22% laboratory) in contrast to monocrystalline cells. Polycrystalline cells exhibit a distinctive blue, mottled appearance resulting from the uneven alignment of crystal grains.



Figure (I.14): Polycrystalline silicon wafer.

I.5.2 Second-Generation Solar Cells.

Second-generation photovoltaic cells are referred to as thin-film cells. Because they use less silicon, they are less expensive than first-generation cells; nevertheless, due to their lesser efficiency, they have a smaller market share. Despite their lower efficiency, thin-film solar cells have been used commercially since 2008.Some advantages of thin film solar cell technology are[21]:

- ✓ Low material consumption.
- ✓ Shorter energy payback period.
- ✓ Monolithic integration.
- ✓ Large area modules.
- ✓ Tenable material properties.
- ✓ Low temperature processes.
- ✓ Transparent modules can be made.

I.5.2.1 Cadmium Telluride (CdTe)

The CdTe modules, whose production reached 5.7 GWp in 2019, are the most effective thin-film photovoltaic technologies now in use. Fast and reliable thin-layer deposition methods and a good fit between the CdTe absorber bandgap and the solar spectrum are two advantages of this technology [25]. The biggest worry with CdTe is the toxicity of cadmium, which requires careful control of manufacturing waste and end-of-life module recycling. Tellurium's limited geological abundance is another possible supply-chain restriction at terawatt sizes.

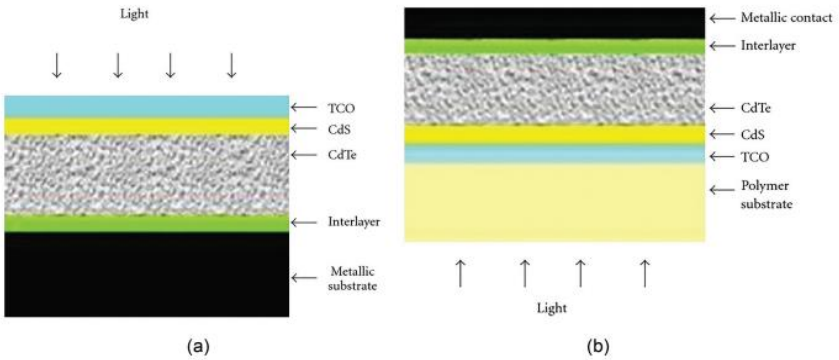


Figure (I.15): Structure of CdTe cell: **(a)** substrate configuration; **(b)** superstrate configuration [25]

I.5.2.2 Copper Indium Gallium Di selenide (CIGS)

Depending on the Ga/In ratio, the tenable direct bandgap of CIGS, a quaternary chalcopyrite semiconductor, ranges from 1.0 eV (CIS) to 1.7 eV (CGS), providing spectrum matching versatility. At 23.35%, CIGS cells hold the record for thin-film efficiency. High-efficiency flexible CIGS modules using polyimide foil have been shown [26]. Process control is difficult due to the complicated quaternary composition, which raises manufacturing costs compared to CdTe. Utility and building-integrated PV applications both use CIGS modules.

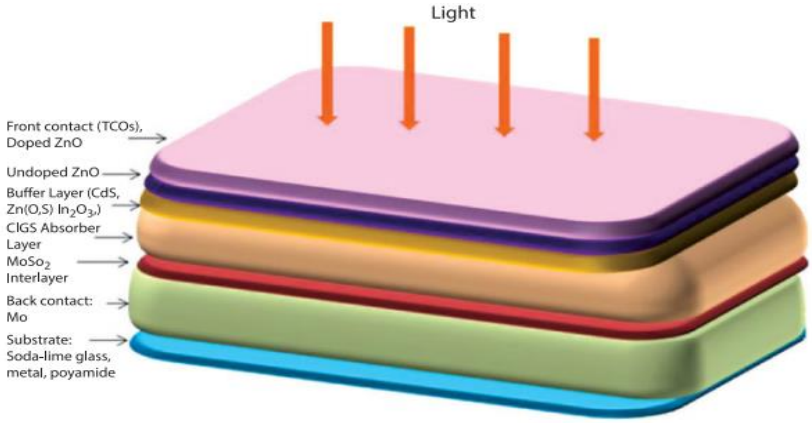


Figure (I.16): Basic structure of typical CIGS solar cell [27]

I.5.3 Third-Generation Solar Cells

Third-generation technologies aim to surpass the Shockley-Queisser single-junction efficiency limit while simultaneously reducing manufacturing costs. They encompass a diverse range of approaches, united by the use of novel materials and physical mechanisms that go beyond the single p-n junction paradigm. First-generation C-Si solar cells and thin-film solar cells are limited in their ability to achieve greater efficiency and establish themselves as photovoltaic technologies [28]. These solar cell types are particularly appealing because to their high conversion efficiency and simple and inexpensive production method.

I.5.3.1 Dye-Sensitized Solar Cells (DSSC)

Brian O'Regan and Michael Grätzel's ground-breaking research on the possible uses of nanosized TiO2 porous film electrodes in dye-sensitized solar cells (DSSC), which use the photoelectric effect to convert solar energy into electricity, marked the beginning of the history of sensitized cells. Due to its low manufacturing costs, environmental friendliness, and high photon-to-electricity conversion efficiency, DSSCs quickly attracted a lot of attention. DSSCs have now achieved an efficiency of about 13% as a result of multiple studies, making them viable options for producing clean and renewable energy [26], [29].

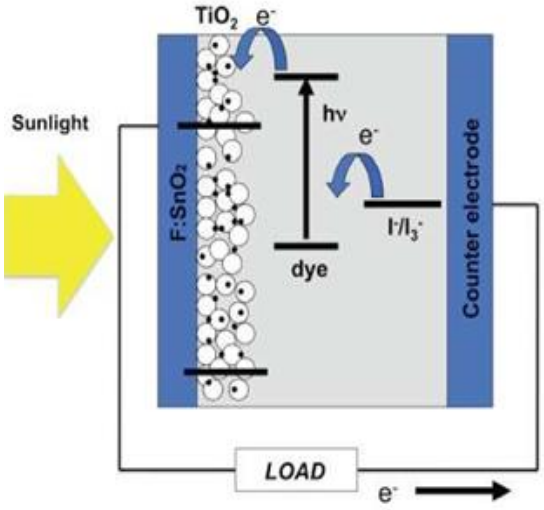


Figure (I.17): Dye sensitized solar cell DSSC diagram [30].

I.5.3.2 Perovskite Solar Cells (PSC)

Recently, organometal trihalide perovskites have shown promise as low-cost, high-efficiency solar cell materials. Because of novel techniques used in their manufacturing process, such as device construction, interfacial engineering, chemical compositional tuning, and crystallization kinetics control, the efficiency of perovskite solar cells (PSC) has been updated quickly in less than five years. The highest PSC efficiency to date is 20.1%, which is comparable to single crystal silicon solar cells [31].

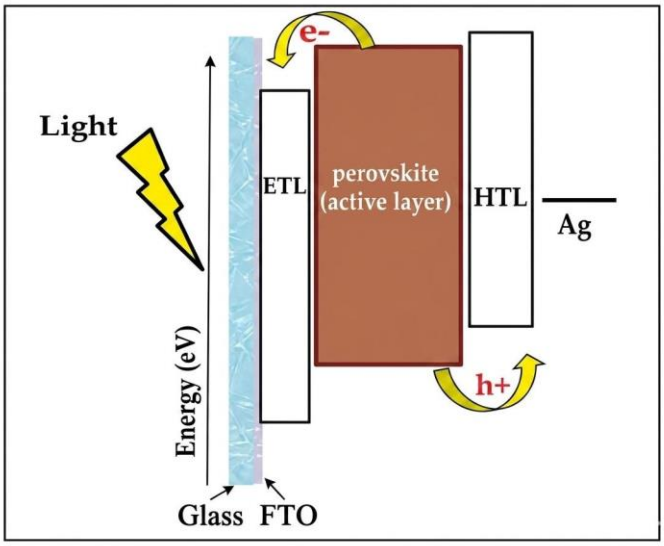


Figure (I.18): Typical structure of a perovskite solar cell [32]

The appeal of PSCs arises from a rare convergence of desirable properties. Metal-halide perovskites exhibit strong optical absorption, low exciton binding energies, long carrier diffusion lengths, and defect tolerance that allows high performance despite solution-based processing. These materials can often be deposited at comparatively low temperatures and on lightweight substrates, which broadens the manufacturing landscape beyond the high-temperature, capital-intensive routes dominant in crystalline-silicon technology. At the same time, their electronic structure supports efficient generation, separation, and extraction of charges through properly engineered transport layers[33], [34]. The primary obstacle preventing PSC devices from being commercialized, however, is their continued lack of stability**.**

I.5.3.3 Organic Photovoltaics (OPV)

Organic photovoltaic (OPV) technology, whose power conversion efficiency (PCE) is fast rising and holds great promise for practical applications, is a feasible choice for utilizing sustainable solar energy. The development of new materials, advances in device processing methods and mix morphology, and a better understanding of device physics have all contributed significantly to the progress of OPV cells during the last 30 years[35]. One of OPV cells' biggest benefits is solution processability, which allows for large-scale production at low cost through scalable printing technologies.

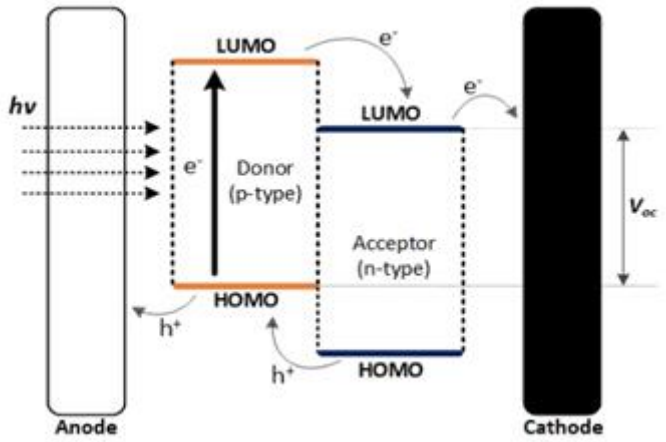


Figure (I.19): OPV's operating principles [10].

I.6 Conclusion

This chapter has provided a comprehensive introduction to the fundamentals of photovoltaic solar cells, spanning the physics of light and solar radiation through cell-level device physics, electrical modelling, and the technological landscape of solar cell generations. The following chapter will concentrate on one example of third-generation solar cells: perovskites. This chapter outlines the key scientific principles behind perovskite materials, including $CsSnGeI_3$, and explains how their crystallographic, optical, and electrical properties impact the performance of solar cells.

Bibliography for Chapter I

[1] N. Chu, P. M.-G. E. N. I. (GENI), S. Diego, undefined CA, and undefined 2011, "Review and comparison of different solar energy technologies," *geni.orgY Chu, P MeisenGlobal Energy Network Institute (GENI), San Diego:* http://www.geni.org/globalenergy/research/review-and-comparison-of-solar-technologies/Review-and-Comparison-of-Different-Solar-Technologies.pdf

[2] S. C. Bhatia, Ed., "Advanced Renewable Energy Systems, (Part 1 and 2)," Apr. 2014, doi: 10.1201/B18242.

[3] "An Assessment of Solar Energy Conversion Technologies and Research Opportunities GCEP Energy Assessment Analysis Summer 2006 Global Climate & Energy Project Technical Assessment Report Issued by the Global Climate and Energy Project", Accessed: May 14, 2026. [Online]. Available: http://gcep.stanford.edu

[4] H. H. Malitson, "The solar electromagnetic radiation environment.," 1968.

[5] T. L. . Brown, H. Eugene. LeMay, B. Edward. Bursten, C. J. . Murphy, P. M. . Woodward, and Matthew. Stoltzfus, "Chemistry : the central science," p. 1083, 2023.

[6] M. Ş. Kalay, B. Kılıç, and Ş. Sağlam, "Systematic review of the data acquisition and monitoring systems of photovoltaic panels and arrays," *Solar Energy*, vol. 244, pp. 47–64, Sep. 2022, doi: 10.1016/J.SOLENER.2022.08.029.

[7] N. Desrues, "Développement de cellules photovoltaïques à hétérojonctions silicium et contacts en face arrière," 2009, Accessed: May 14, 2026. [Online]. Available: https://theses.fr/2009ISAL0084

[8] G. W. Crabtree and N. S. Lewis, "Solar energy conversion," *Phys. Today*, vol. 60, no. 3, pp. 37–42, 2007, doi: 10.1063/1.2718755.

[9] K. K. Jaiswal *et al.*, "Renewable and sustainable clean energy development and impact on social, economic, and environmental health," *Energy Nexus*, vol. 7, p. 100118, Sep. 2022, doi: 10.1016/J.NEXUS.2022.100118.

[10] E. K. Solak and E. Irmak, "Advances in organic photovoltaic cells: a comprehensive review of materials, technologies, and performance," *RSC Adv.*, vol. 13, no. 18, pp. 12244–12269, Apr. 2023, doi: 10.1039/D3RA01454A.

[11] N. Guerra, M. Guevara, C. Palacios, and F. Crupi, "Operation and physics of photovoltaic solar cells: an overview," *I+D Tecnológico*, vol. 14, no. 2, pp. 84–95, Dec. 2018, doi: 10.33412/IDT.V14.2.2077.

[12] M. C. Scharber and N. S. Sarciftci, "Bulk Heterojunction Organic Solar Cells: Working Principles and Power Conversion Efficiencies," *RSC Nanoscience and Nanotechnology*, vol. 2018-January, no. 45, pp. 33–68, Nov. 2017, doi: 10.1039/9781782626749-00033.

[13] N. Gundogdu, M. Akkus, M. O.-S. U. J. of, and undefined 2021, "Investigation of basic principles and technologies of solar cells," *sujes.selcuk.edu.trK Gundogdu, MS Akkus, MT OzelSelcuk University Journal of Engineering Sciences, 2021•sujes.selcuk.edu.tr*, vol. 20, no. 02, pp. 50–55, 2021, Accessed: May 14, 2026. [Online]. Available: https://sujes.selcuk.edu.tr/sujes/article/view/540

[14] A. Khatibi, F. Razi Astaraei, and M. H. Ahmadi, "Generation and combination of the solar cells: A current model review," *Energy Sci. Eng.*, vol. 7, no. 2, pp. 305–322, Apr. 2019, doi: 10.1002/ESE3.292;WGROUP:STRING:PUBLICATION.

[15] W. W. B. Bonkoungou, Z. Koalaga, and D. Njomo, "Modelling and simulation of photovoltaic module considering single-diode equivalent circuit model in MATLAB," Int. J. Emerg. Technol. Adv. Eng., vol. 3, no. 3, pp. 493–502, 2013.

[16] E. Cuce, P. M. Cuce, I. H. Karakas, and T. Bali, "An accurate model for photovoltaic (PV) modules to determine electrical characteristics and thermodynamic performance parameters," *Energy Convers. Manag.*, vol. 146, pp. 205–216, 2017, doi: 10.1016/j.enconman.2017.05.022.

[17] S. F. Shaikh *et al.*, "Nanostructures in Dye-Sensitized and Perovskite Solar Cells," *Nanostructures*, Mar. 2019, doi: 10.5772/INTECHOPEN.83803.

[18] S. A. Afghan, H. Almusawi, and H. Geza, "Simulating the electrical characteristics of a photovoltaic cell based on a single-diode equivalent circuit model," *MATEC Web of Conferences*, vol. 126, Oct. 2017, doi: 10.1051/MATECCONF/201712603002.

[19] A. Blakers, N. Zin, K. R. McIntosh, and K. Fong, "High Efficiency Silicon Solar Cells," *Energy Procedia*, vol. 33, pp. 1–10, 2013, doi: 10.1016/J.EGYPRO.2013.05.033.

[20] A. Goetzberger and C. Hebling, "Photovoltaic materials, past, present, future," *Solar Energy Materials and Solar Cells*, vol. 62, no. 1, pp. 1–19, Apr. 2000, doi: 10.1016/S0927-0248(99)00131-2.

[21] M. V. Dambhare, B. Butey, and S. V. Moharil, "Solar photovoltaic technology: A review of different types of solar cells and its future trends," *J. Phys. Conf. Ser.*, vol. 1913, no. 1, p. 012053, May 2021, doi: 10.1088/1742-6596/1913/1/012053.

[22] M. B. Hayat, D. Ali, K. C. Monyake, L. Alagha, and N. Ahmed, "Solar energy—A look into power generation, challenges, and a solar-powered future," *Int. J. Energy Res.*, vol. 43, no. 3, pp. 1049–1067, Mar. 2019, doi: 10.1002/ER.4252;CTYPE:STRING:JOURNAL.

[23] N. Wang *et al.*, "Heterojunction-Depleted Lead-Free Perovskite Solar Cells with Coarse-Grained B-γ-CsSnI3 Thin Films," *Adv. Energy Mater.*, vol. 6, no. 24, p. 1601130, Dec. 2016, doi: 10.1002/AENM.201601130;WGROUP:STRING:PUBLICATION.

[24] F. Shimura, "Single-crystal silicon: growth and properties," *Springer Handbooks*, p. 1, 2017, doi: 10.1007/978-3-319-48933-9_13/SAVE-RESEARCH.

[25] A. Zdyb, "Third generation solar cells," *Third Generation Solar Cells*, Nov. 2023, doi: 10.1201/9781003196785.

[26] B. O'Regan and M. Grätzel, "A low-cost, high-efficiency solar cell based on dye-sensitized colloidal TiO2 films," *Nature 1991 353:6346*, vol. 353, no. 6346, pp. 737–740, Oct. 1991, doi: 10.1038/353737a0.

[27] R. Mohan and R. Paulose, "Brief review on copper indium gallium diselenide (CIGS) solar cells," *Photoenergy and Thin Film Materials*, pp. 157–192, Mar. 2019, doi: 10.1002/9781119580546.CH4.

[28] A. Kojima, K. Teshima, Y. Shirai, and T. Miyasaka, "Organometal Halide Perovskites as Visible-Light Sensitizers for Photovoltaic Cells," *J. Am. Chem. Soc.*, vol. 131, no. 17, pp. 6050–6051, May 2009, doi: 10.1021/JA809598R.

[29] J. A. Castillo-Robles, E. Rocha-Rangel, J. A. Ramírez-De-león, F. C. Caballero-Rico, and E. N. Armendáriz-Mireles, "Advances on Dye-Sensitized Solar Cells (DSSCs) Nanostructures and Natural Colorants: A Review," *Journal of Composites Science 2021, Vol. 5*, vol. 5, no. 11, Oct. 2021, doi: 10.3390/JCS5110288.

[30] N. Alhamed, A. Issa, A. D.-J. of electron Devices, and undefined 2012, "Studying of natural dyes properties as photo-sensitizer for dye sensitized solar cells (DSSC)," *academia.eduM Alhamed, AS Issa, AW DoubalJournal of electron Devices, 2012•academia.edu*, Accessed: May 15, 2026. [Online]. Available: https://www.academia.edu/download/76910797/16_Mounir.pdf

[31] 7.677Q1SJR Q1; 7.677NAABS NANAABDC NAAdvanced Energy MaterialsNH Tiep, Z. Ku, H. F.-A. E. Materials, and undefined 2016,

[32] P. Basumatary and P. Agarwal, "A short review on progress in perovskite solar cells," *Mater. Res. Bull.*, vol. 149, p. 111700, May 2022, doi: 10.1016/J.MATERRESBULL.2021.111700.

[33] L. Zhang, Y. Zhao, and Q. Dai, "Recent Progress in Perovskite Solar Cell: Fabrication, Efficiency, and Stability," *Challenges and Advances in Computational Chemistry and Physics*, vol. 32, pp. 1–32, 2021, doi: 10.1007/978-3-030-69445-6_1.

[34] P. Roy, A. Ghosh, F. Barclay, A. Khare, and E. Cuce, "Perovskite Solar Cells: A Review of the Recent Advances," *Coatings 2022, Vol. 12*, vol. 12, no. 8, Jul. 2022, doi: 10.3390/COATINGS12081089.

[35] L. Zhu *et al.*, "Progress of organic photovoltaics towards 20% efficiency," *Nature Reviews Electrical Engineering*, vol. 1, no. 9, pp. 581–596, Aug. 2024, doi: 10.1038/S44287-000080-3

[36] Jaiswal, K. K., Chowdhury, C. R., Yadav, D., Verma, R., Dutta, S., Jaiswal, K. S., & Karuppasamy, K. S. K. (2022). Renewable and sustainable clean energy development and impact on social, economic, and environmental health. *Energy nexus*, *7*, 100118.

Chapter II: Perovskite Solar Cells

II.1 Introduction

The advent of perovskite solar cells represents a paradigm shift in the field of photovoltaics. Historically dominated by crystalline silicon, the PV market has continuously sought alternatives that could deliver comparable or superior efficiencies while mitigating the high manufacturing costs and energy-intensive processing associated with silicon wafers**.**

This chapter comprehensively details the foundational science of perovskite materials, tracking their application in solar cell devices. We elucidate the crystallographic, optical, and electrical fundamentals that dictate device performance. A significant portion of this discourse is dedicated to classifying modern perovskite materials, ultimately focusing on the critical frontier of lead-free formulations. Specifically, we explore the theoretical and simulated potential of the inorganic, lead-free alloy $CsSnGeI_3$, assessing its composition, phase stability, and operational mechanics. By addressing current challenges and surveying recent structural innovations, this text establishes a holistic understanding of the future trajectory of sustainable perovskite photovoltaics

II.2 Fundamentals of Perovskite Materials

II.2.1 Definition of Perovskite Materials

The mineral calcium titanate ($CaTiO_3$), named for the Russian mineralogist Lev Perovski and found in the Ural Mountains in 1839 by Gustav Rose, was the first mineral to be referred to as "perovskite". The nomenclature used in solid-state chemistry and materials research nowadays can refer to any synthesized or naturally occurring molecule that shares the same basic crystallographic structure as $CaTiO_3$ [1]. Two The general ABX_3 stoichiometry, in which 'A' and 'B' stand for two separate cation species with noticeably different sizes and 'X' is the anion that bonds to both, is what distinguishes a perovskite.

II.2.2 Crystal Structure of Perovskites

The crystal chemistry of perovskites provides the conceptual foundation for understanding their behaviour as solar absorbers. In its idealized form, the ABX3 perovskite lattice consists of corner-sharing BX6 octahedra, which define a three-dimensional framework, while the A-site cation occupies the cuboctahedral cavity created by that framework. In oxide perovskites X is typically oxygen; in photovoltaic metal-halide perovskites X is commonly I−, Br−, or Cl−. The B-site cation is usually Pb2+, Sn2+, Ge2+, or a metal combination, whereas the A-site may be a 4 organic cation such as methylammonium (MA+) or formamidinium (FA+), or an inorganic cation such as Cs+ [2], [3].

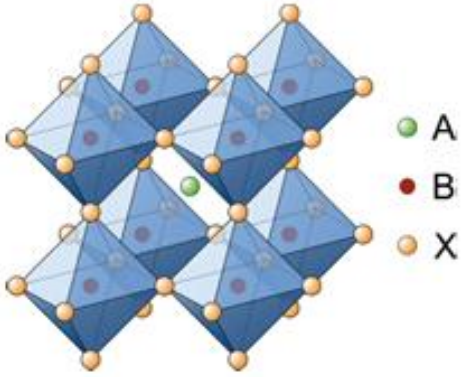


Figure (II.1): Generic ABX_3 metal-halide perovskite framework and octahedral connectivity [4].

The stability and formability of this crystal lattice are largely determined by the geometric limitations included in the Goldschmidt tolerance factor (t) and the octahedral factor (μ). The tolerance factor is mathematically expressed as:

$$\mu = \frac{r_B}{r_X} \qquad \text{(II. 1)}$$

$$t = \frac{(r_A + r_X)}{\sqrt{2}(r_B + r_X)} \qquad \text{(II. 2)}$$

The ionic radii of the respective component ions are denoted by $\boldsymbol{r_A}$, $\boldsymbol{r_B}$, and $\boldsymbol{r_X}$. Although these parameters are approximate and especially imperfect when molecular cations occupy the A-site, they remain useful heuristics for anticipating whether a given ionic combination can adopt a three-dimensional perovskite framework. Becker, Klüner, and Wark showed that tolerance-factor analysis remains a valuable guide in screening ABX3 combinations for solar-cell applications, while also cautioning that estimating effective radii for molecular cations is not trivial [3].

II.2.3 Structural Properties of Perovskites

The stability and formability of the ABX_3 perovskite lattice is empirically predicted using the Goldschmidt tolerance factor (t) and the octahedral factor (μ). The tolerance factor evaluates the geometric fit of the constituent ions and is defined as the ratio of the sum of the ionic radii of the A and X ions to the square root of two times the sum of the ionic radii of the B and X ions. A perfect cubic structure is generally realized when the tolerance factor is approximately 1. However, stable perovskite phases can form within a range of roughly 0.8 to 1.1. If the 'A' cation is too small, the BX_6 octahedra tilt to accommodate the void, resulting in lower symmetry structures such as tetragonal or orthorhombic phases. If the 'A' cation is too large, the three-

dimensional corner-sharing network breaks down, leading to the formation of two-dimensional or one-dimensional structures [5].

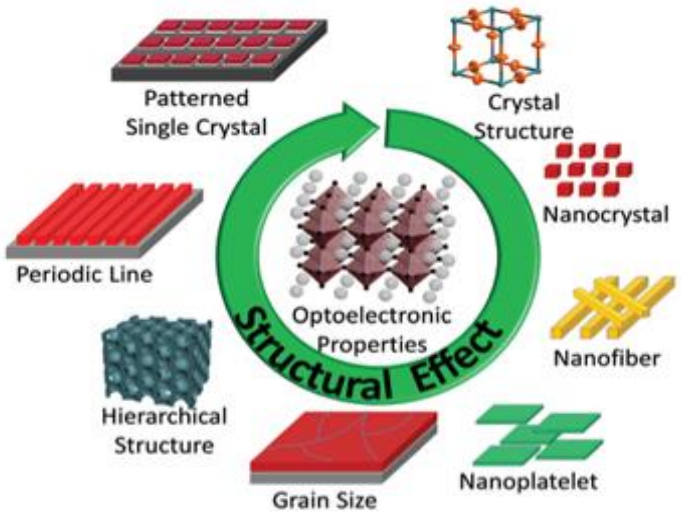


Figure (II.2): the main structural elements that affect halide perovskites' characteristics [6].

A further significant structural attribute is their tolerance to defects. In stark contrast to conventional covalent semiconductors, such as silicon or gallium arsenide, which are highly susceptible to crystallographic defects that function as deep-level trap states facilitating non-radiative recombination, halide perovskites demonstrate remarkable defect tolerance. The pronounced ionic character of their lattice, combined with the specific atomic orbital contributions at the band edges, is understood to ensure that thermodynamically favoured defects, for instance, halide vacancies, typically yield shallow transition levels proximate to either the conduction or valence bands, rather than generating deep trap states within the mid-gap region. This mechanism consequently enables perovskite films, even when fabricated via comparatively simple, low-temperature solution-based processes, to maintain exceptionally low non-radiative recombination rates, which serves as a key indicator of their high efficiency[7], [8].

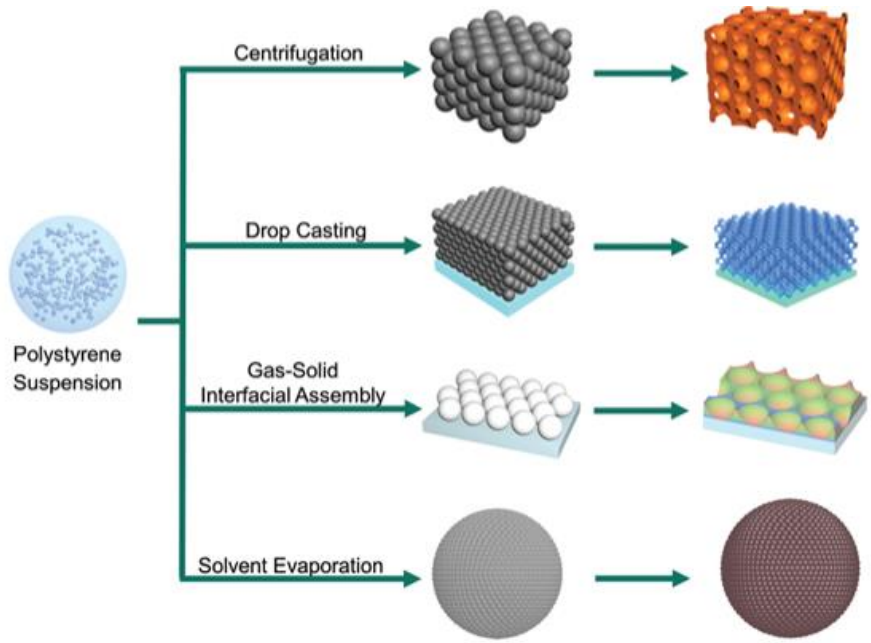


Figure (II.3): The methods for producing artificial templates and halide perovskite

II.3 Perovskite Solar Cells

II.3.1 Operating Principle

Using the perovskite material as the main photoactive absorber, a perovskite solar cell operates on the basis of the photovoltaic effect. Electrons from the valence band are excited when photons from incident sunlight with energy equal to or higher than the bandgap hit the perovskite layer. The band of conduction. The resulting excitons (bound electron-hole pairs) spontaneously dissociate into free charge carriers' free electrons and holes almost instantly upon generation because metal halide perovskites have low exciton binding energies (usually in the range of a few millielectronvolts at room temperature) [9],[10].

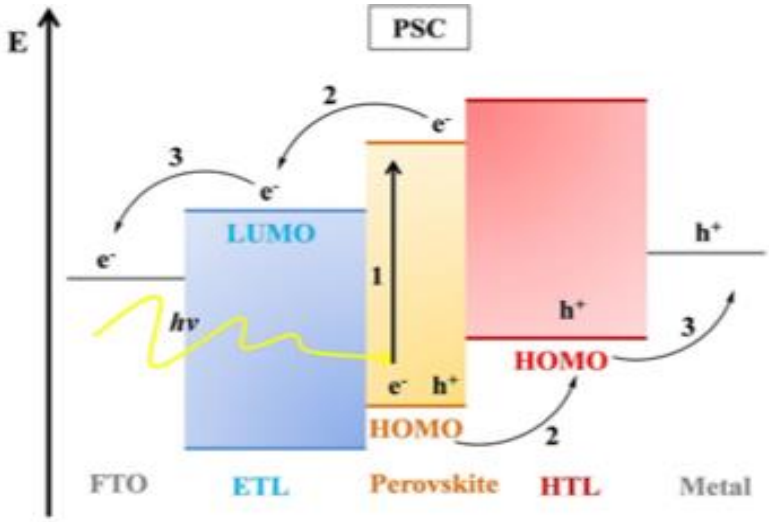


Figure (II.4): Band diagram and operating principle of a perovskite solar cell [11].

In order to minimize carrier recombination at the interfaces and maximize the open circuit voltage (Voc) of the device, these free carriers must be quickly extracted before they recombine. The internal electric field created by the energetic differences between the adjacent charge-transporting layers provides the driving force. Electrons are swept toward the Electron Transport Layer (ETL), while holes are driven in the opposite direction toward the Hole Transport Layer (HTL). The carriers eventually reach the corresponding current-collecting electrodes (the transparent conductive oxide anode and the metal cathode) [12].

II.3.2 Device Architecture

The structural evolution of PSCs has yielded a variety of device architectures, designed to optimize charge extraction, ease of manufacturing, and long-term stability. The earliest perovskite cells evolved from dye sensitized solar cells (DSSCs) and therefore utilized a mesoscopic architecture. Over time, as the excellent intrinsic transport properties of perovskites were fully realized, researchers developed simpler, planar architectures.

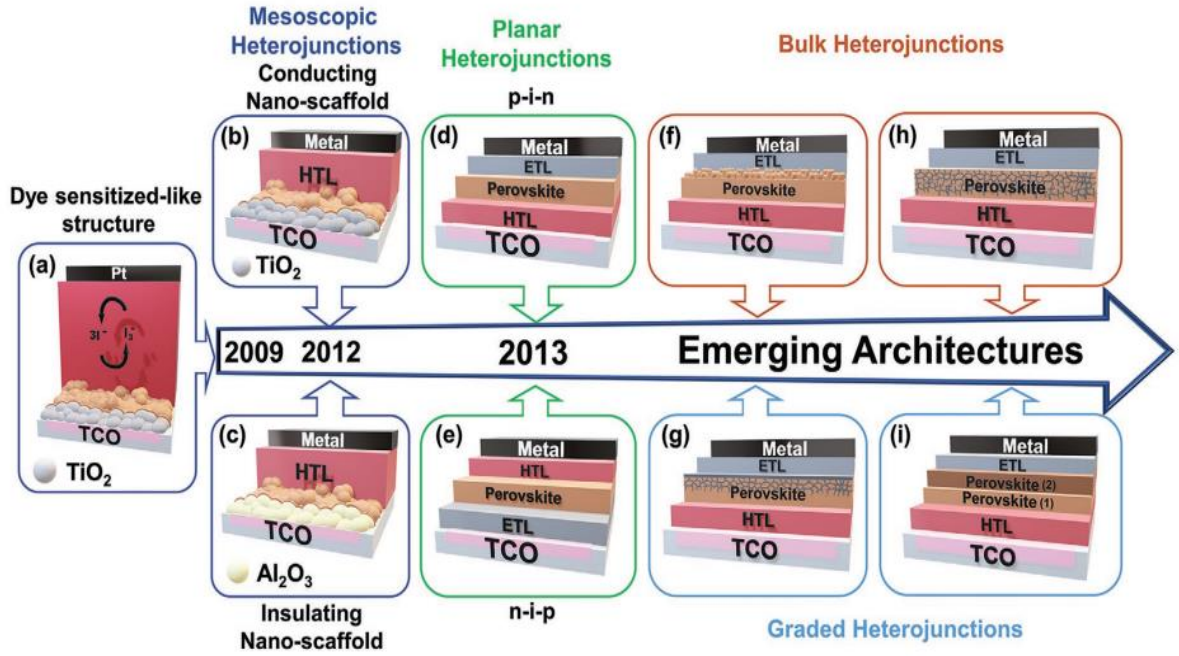


Figure (II.5): A chronology of the evolution of perovskite solar cells from conventional to novel designs [13].

In general, the order in which the light-harvesting and transport layers are applied to the transparent

substrate determines the classification of device architectures [11]:

- **n-i-p (Regular) Structure:** An n-type electron transport layer (usually TiO_2 or SnO_2). This can be a purely planar shape or a mesoporous form, where a scaffold of nanoparticles offers a large surface area for perovskite infiltration. A p-type hole transport layer (such Spiro-OMeTAD or PTAA) and a metal back contact come after the perovskite layer, which serves as the intrinsic (i) absorber.
- **p-i-n (Inverted) Structure:** In this configuration, derived primarily from organic photovoltaics, light enters through a p-type hole transport layer (e.g., NiOx or PEDOT: PSS). The perovskite is sandwiched between this HTL and an overlaid ETL (frequently PCBM or C_{60}). The inverted structure typically displays less J-V hysteresis and is highly compatible with low-temperature processing and flexible substrates.
- **ETL/HTL-Free Architectures:** To reduce fabrication costs and complexity, simplified architectures have been proposed wherein either the ETL or the HTL is entirely omitted. These designs rely heavily on the ambipolar transport capacity of the perovskite itself and meticulous interface engineering to prevent recombination at the bare electrode interfaces.

II.3.3 Charge Transport Mécanisme

Efficient charge transport is the fulcrum upon which PSC performance balances. The fundamental mechanisms involve carrier diffusion and drift within the perovskite bulk, followed by carrier transfer across the heterointerfaces. Within the bulk, the mobility of carriers is influenced by electron-phonon coupling; specifically, the interaction between charge carriers and the dynamic lattice vibrations of the inorganic framework (often resulting in polaron formation). This large-polaron mechanism is hypothesized to screen carriers from charged defects, contributing to the phenomenally low recombination rates observed.

However, actual device efficiency is severely constrained by interface dynamics. Once charge carriers pass through the boundaries of the perovskite film, they proceed to the ETL and HTL. If the HTL's valence band maximum and the ETL's conduction band lowest energy levels are not in good alignment with energy barriers that keep the perovskite from being extracted. Shockley-Read-Hall (SRH) non-radiative recombination can also be caused by structural or chemical defects at these interfaces, such as uncoordinated lead or halide vacancies, which can act as deep traps. Advanced passivation techniques using organic molecules or low-dimensional (2D) perovskite capping layers are commonly employed to permit rapid and loss-free charge transfer across the device cross-section[14],[15].

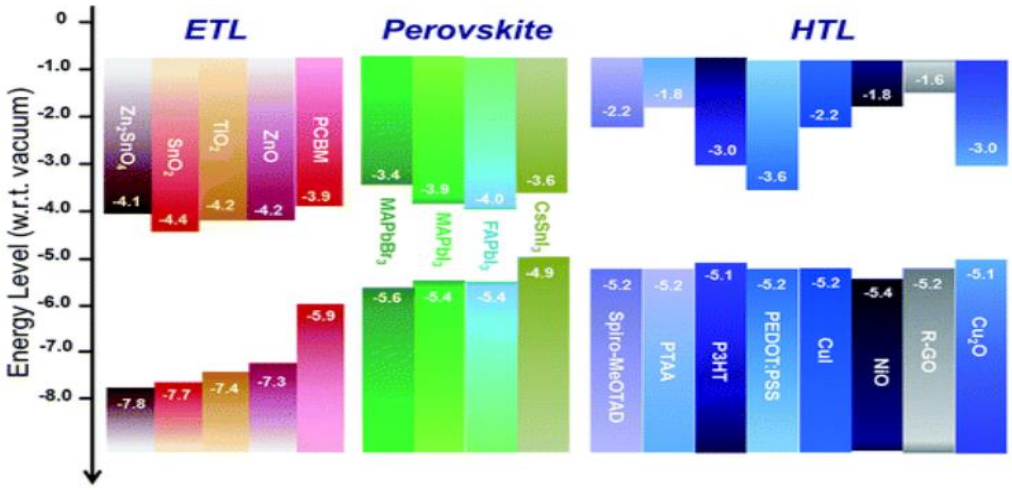


Figure (II.6): An example of literature values for the energy levels in relation to the vacuum level of several materials that function as hole-selective layers (right), electron-selective layers (left), and perovskite absorbers in perovskite solar cell [16].

II.4 Physical and Electronic Properties of Perovskite Materials

The remarkable performance metrics of perovskite solar cells are deeply intertwined with their intrinsic physical and electronic properties. The atomic composition and the resulting

orbital hybridization determines the energetic landscape of the material, which governs how it interacts with light and electricity.

II.4.1 Band Gap Energy

The band gap energy (Eg) is the most critical parameter for any photovoltaic absorber, as it determines both the maximum possible short-circuit current density (Jsc) and the open-circuit voltage (Voc) according to the Shockley-Queisser detailed balance limit. The ideal band gap for a single-junction solar cell under the standard AM1.5G solar spectrum is approximately 1.34 eV. One of the most celebrated features of halide perovskites is their widely tenable band gap. By altering the stoichiometric ratio of the halides (e.g., mixing iodine and bromine) or substituting the cations at the A or B sites, the band gap can be continuously tuned from about 1.2 eV to over 3.0 eV. For instance, partial substitution of Pb with Sn in $MAPbI_3$ reduces the band gap closer to the ideal limit, while incorporating Br increases it, which is highly advantageous for developing tandem solar cells with silicon or CIGS bottom cells [17].

II.4.2 Absorption Coefficient

As previously mentioned, perovskite materials exhibit extremely high optical absorption coefficients, frequently exceeding 10^5 cm^{-1} in the visible light spectrum. This high coefficient originates from the direct p-p electronic transitions between the filled valence band, primarily composed of halide p-orbitals and metal s-orbitals, and the empty conduction band, derived mainly from metal p-orbitals. Consequently, an ultra-thin perovskite layer of roughly 300 to 500 nanometres is capable of absorbing over 90% of incident photons above the band gap energy. This not only minimizes the material consumption required for device fabrication but also reduces the distance charge carriers must travel to reach the transport layers, thereby decreasing the probability of bulk recombination[18].

II.4.3 Carrier Mobility

High carrier mobility is essential for efficient charge extraction. The high mobilities observed in perovskite single crystals and high-quality polycrystalline films are attributed to the low effective masses of both electrons and holes at the band edges. The spatial overlap of the expansive metal p-orbitals and halide p-orbitals in the corner-sharing octahedral network facilitates significant electronic delocalization, allowing charge carriers to move through the lattice with high velocity under an electric field. The combination of high carrier mobility and long carrier lifetimes (often extending into the microsecond regime) yields exceptionally long diffusion lengths. In certain highly crystalline, defect-passivated films, these diffusion lengths can exceed 3 micrometres, ensuring that practically all photogenerated carriers are successfully

collected by the selective contacts before recombination occurs [19].

II.5 Classification of Perovskite Materials

Perovskite absorbers used in solar cells can be grouped into three broad classes: organic-inorganic hybrid perovskites, all-inorganic perovskites, and lead-free perovskite materials. These families are related by a common structural logic yet differ markedly in thermal behaviour, environmental sensitivity, toxicity profile, and current efficiency ceiling.

II.5.1 Organic–Inorganic Perovskites

Organic-inorganic hybrid perovskites remain the most extensively studied and the most successful in terms of record efficiencies. In these materials the A-site is occupied by an organic cation such as methylammonium (MA+) or formamidinium (FA+), while the B-site is often Pb2+ and the X-site consists of iodide, bromide, chloride, or a mixture of halides. Famous examples include MAPbI3, FAPbI3, and mixed-cation mixed-halide compounds based on FA/MA/Cs with Pb (I, Br)3 frameworks. Their appeal lies in excellent optoelectronic quality, ease of processing, and powerful compositional tunability [2],[20].

Hybrid perovskites often display superior photovoltaic performance because their band gaps can be tuned with great precision and because extensive defect-passivation strategies have been developed for them. Mixed-cation formulations suppress the phase instability associated with pure FAPbI3, while mixed halides enable wider band gaps for tandem cells. However, the organic cations also introduce vulnerabilities. Volatility, hygroscopicity, and thermal fragility contribute to degradation pathways under heat and moisture. Consequently, the highest efficiencies in this family have not eliminated ongoing concerns about operational durability [21],[22].

II.5.2 Inorganic Perovskites

Fully inorganic perovskites substitute an inorganic alkali metal, nearly always cesium (Cs), for the A-site molecule in order to totally eliminate the heat and moisture instability caused by organic cations. With a bandgap of about 1.7 eV, cesium lead iodide ($CsPbI_3$) is quite appealing for the top cell of tandem photovoltaic systems. These films can withstand continuous heat stress above 300°C because the removal of volatile organic molecules significantly increases the material's intrinsic thermal endurance.

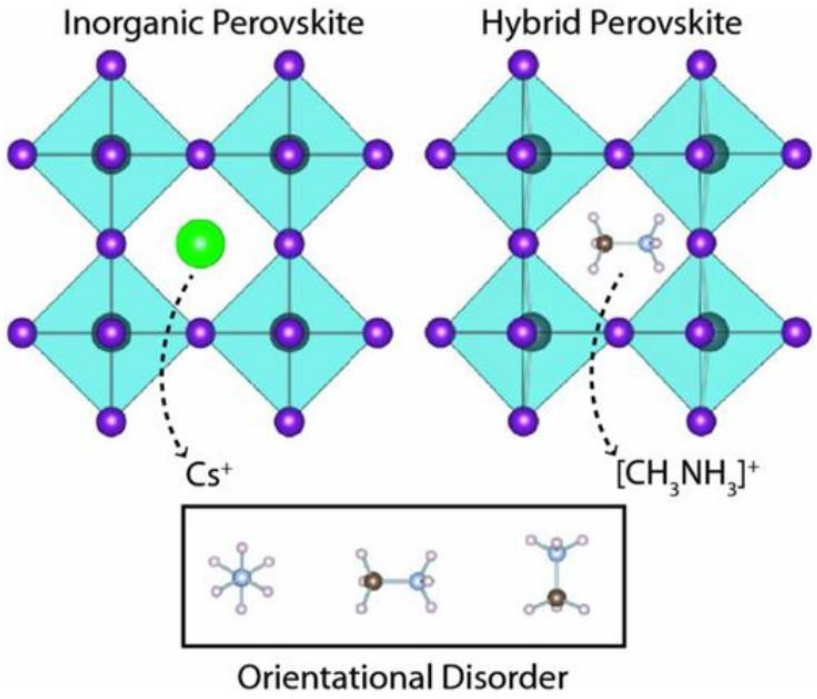


Figure (II.7): Illustration of the perovskite structure based on corner sharing octahedra of BX6 with either a monovalent metal (inorganic) or charged molecule (hybrid) at the centre of the unit cell.

Nevertheless, purely inorganic perovskites confront severe phase stability dilemmas. At room temperature, the cubic perovskite phase of $CsPbI_3$ is thermodynamically metastable and rapidly collapses into an orthorhombic non-perovskite phase lacking photovoltaic activity. Intensive research efforts, including strain engineering, the incorporation of stabilizing quantum dots, and partial substitution of the halide anions, are deployed to preserve the functional crystalline structure in ambient operating environments [23],[24].

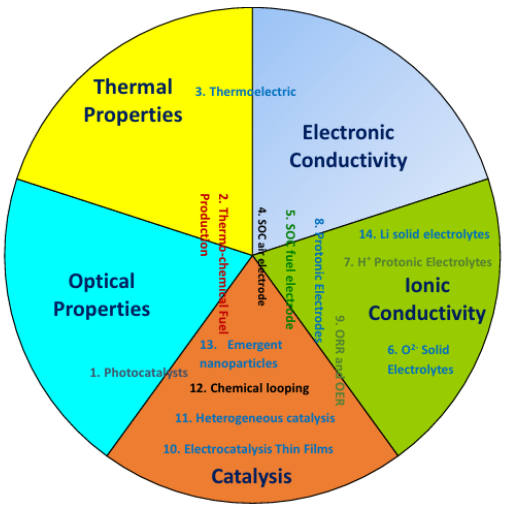


Figure (II.8): Scheme for Inorganic Perovskites for Energy Applications [25].

II.5.3 Lead-Free Materials

Lead-free perovskite materials constitute a third and particularly active field because they respond to environmental and regulatory concerns surrounding lead. The most prominent B-site alternatives are tin, germanium, bismuth, antimony, silver-bismuth double-perovskite combinations, and mixed-metal systems. Among these, Sn-based and Sn/Ge-based perovskites are especially important because they can preserve a three-dimensional perovskite framework and offer band gaps compatible with photovoltaic absorption [26],[27].

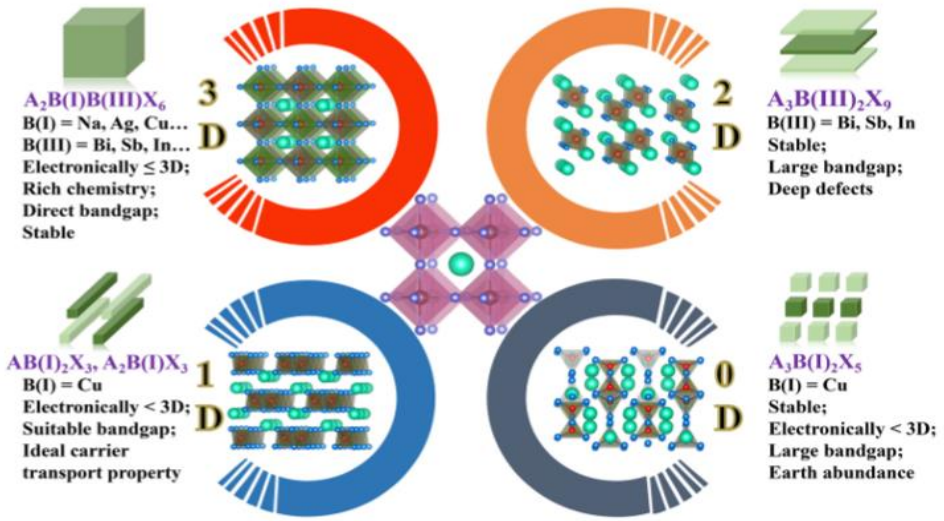


Figure (II.9): Schematic illustration of conventional 3D perovskites and four representative lead-free perovskites or perovskite derivatives with different dimensions in structure and morphology levels [28].

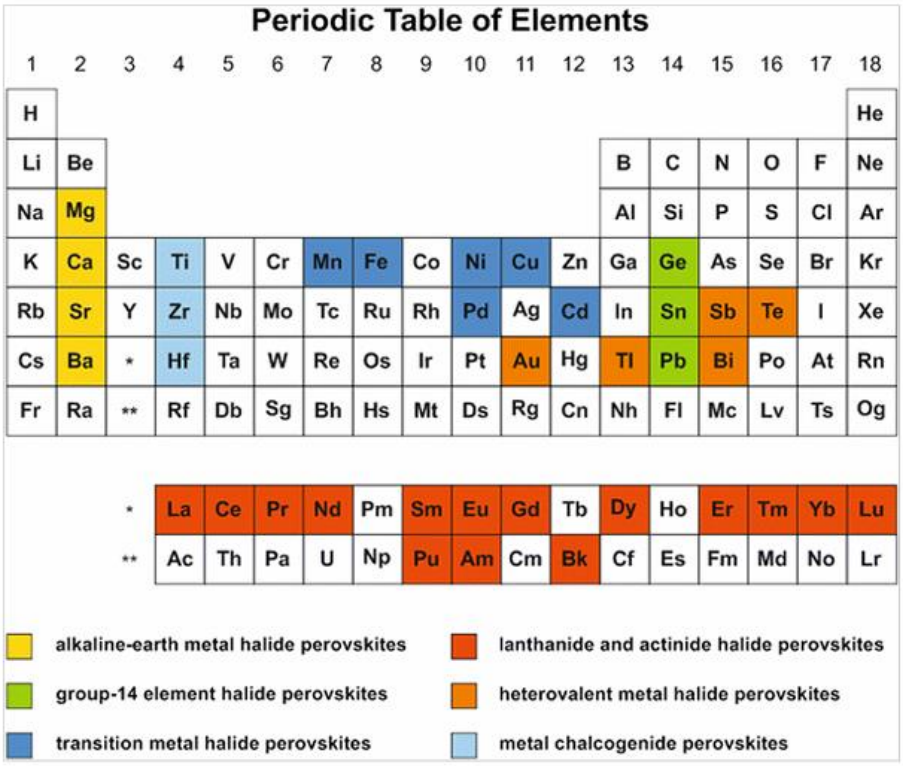


Figure (II.9): Candidate elements for lead replacement in perovskite-type compounds [4].

Among candidates for monovalent substitution, Group-14 elements such as tin (Sn^{2+}) and germanium (Ge^{2+}) are the most logical successors due to their similar ionic radii and outermost s-orbital electron configurations, which theoretically mirror the favourable optoelectronic behaviour of lead. Tin-based perovskites ($FASnI_3$, $CsSnI_3$) display excellent charge mobility and narrower bandgaps, rendering them highly suited for near-infrared harvesting. However, the Achilles heel of both Sn^{2+} and Ge^{2+} lies in the inert pair effect; they are highly susceptible to spontaneous oxidation into their +4 states (Sn^{4+} and Ge^{4+}) upon exposure to trace amounts of oxygen. This oxidation obliterates the crystalline structure and introduces massive p-type self-doping, effectively short-circuiting the solar cell. Consequently, modern research focuses intensely on exploring alloyed systems and complex interface management to mitigate these vulnerabilities[4].

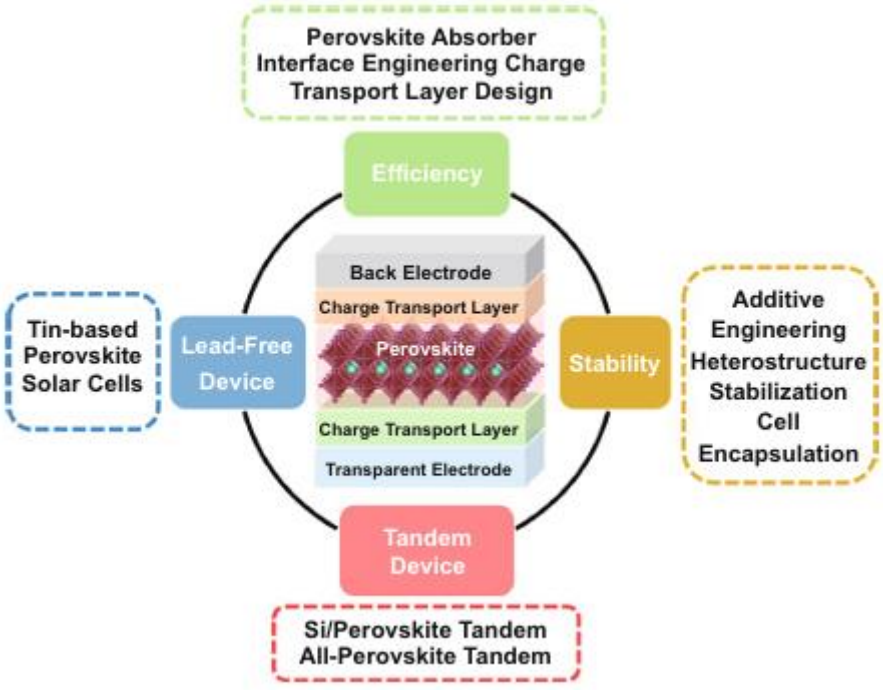


Figure (II.10): Schematic Illustration of Efficiency and Stability Enhancement Strategies in Lead-Free Perovskite Solar Cells [29].

II.6 Lead-Free Perovskite Absorber Material: $CsSnGeI_3$

II.6.1 Chemical Composition of $CsSnGeI_3$

In the pursuit of stable and efficient lead-free alternatives, multi-metal alloying has emerged as a robust strategy. Cesium tin-germanium triiodide ($CsSnGeI_3$) represents a highly promising fully inorganic, mixed B site perovskite. By co-alloying tin and germanium at the octahedral centre, researchers aim to harness a synergistic balance. While pure $CsSnI_3$ demonstrates favourable bandgaps but extreme sensitivity to oxidation, and pure $CsGeI_3$ suffers from severe morphological and stability issues owing to the even smaller ionic radius of germanium, the solid solution $CsSnGeI_3$ creates an intermediate crystallographic landscape.

The chemical composition incorporates an inorganic cesium A-site cation, maximizing fundamental thermal resilience, while the varying molar ratios of Sn and Ge on the B-site allow for the precise calibration of lattice strain and electronic band structure. Such compositional tuning has been reported to substantially increase the formation energy of the problematic Sn^{4+} oxidation state, thereby imparting enhanced ambient stability compared to non-alloyed tin equivalents [30],[31].

II.6.2 Structural Properties

Crystallographic ally, the introduction of germanium into the tin-iodide lattice manipulates the Goldschmidt tolerance factor and influences the [BX_6] octahedral tilting. Because the Ge^{2+} ion is notably smaller than the Sn^{2+} ion, its incorporation induces a slight lattice contraction. Simulated structural analyses and preliminary empirical data suggest that an optimized Sn:Ge ratio stabilizes a higher-symmetry framework at standard operating conditions, which is crucial for isotropic charge transport. Furthermore, the robust inorganic nature of the Cs^+ cation prevents the entropic disorder frequently associated with rotating organic dipoles like methylammonium, leading to a rigid and reliable three-dimensional crystal network that is less susceptible to thermal degradation [30],[32].

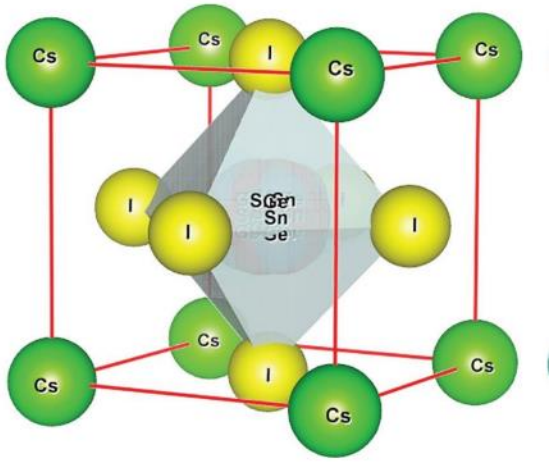


Figure (II.11): The crystal structure of CsSnGeI3 [33].

II.6.3 Optical Properties

For solar absorption, $CsSnGeI_3$'s optical characteristic is quite beneficial. The material has a direct bandgap estimated at about 1.50 eV, according to theoretical calculations and simulation data. This value allows for excellent absorption of the solar irradiance spectrum from the visible to the near-infrared range since it is extremely close to the single-junction theoretical ideal required by the Shockley-Queisser limit.

Furthermore, $CsSnGeI_3$ exhibits an exceptionally high optical absorption coefficient, approximately 10^1 cm^{-1}.This suggests that the great majority of incoming photons can be captured by an incredibly small layer of the absorber, usually less than one millimetre. In addition to lowering material costs, this thin-film requirement This immediately reduces recombination losses by reducing the distance produced charge carriers must travel to reach the extraction interfaces.

II.6.4 Electrical Properties

The electrical properties of $CsSnGeI_3$, as elucidated predominantly through device simulation modelling via platforms like SCAPS-1D, underscore its massive theoretical potential. The simulated charge carrier mobilities are exceptionally high; literature reports indicate theoretical electron mobilities reaching up to 974 $cm^2/V{\cdot}s$ and hole mobilities around 213 $cm^2/V{\cdot}s$ [34].Such robust mobility figures indicate that free charges can navigate the bulk of the material swiftly, outpacing the rates of internal non-radiative recombination.

Numerical models indicate that $CsSnGeI_3$ solar cells might theoretically attain power conversion efficiencies above 30% when placed in an optimal device configuration, such as using SnO_2 or SnS_2 as an electron transport layer and Cu_2O as a hole transport layer. These models forecast high open circuit voltages (~1.2 V) and fill factors that are close to 90%, as long as bulk defect levels are tightly regulated. It should be made clear, nonetheless, that these remarkable electrical standards are still mostly found in the fields of theoretical prediction and numerical simulation. For continued physical manufacturing, bridging the gap between these simulated boundaries and empirical reality continues to be a major difficulty [35].

II.6.5 Stability of $CsSnGeI_3$

Stability is the ultimate metric for lead-free perovskite viability. The Sn^{2+} to Sn^{4+} oxidation process has historically thwarted the progression of tin-based PVs. The oxidation kinetics are significantly changed by alloying germanium. According to theoretical models, germanium acts as an intrinsic thermodynamic buffer against oxygen infiltration and lattice deterioration by modulating the Fermi level and changing the defect formation energies.

Because $CsSnGeI_3$ is an all-inorganic molecule, it naturally avoids the heat volatilization that affects hybrid organic-inorganic perovskites. Prototype $CsSnGeI_3$ films exhibit remarkable air stability in comparison to pure $CsSnI_3$, according to experimental investigations. The material maintains its structural integrity and optical characteristics over prolonged ambient exposure without the abrupt onset of metallic behaviour brought on by p-type self-doping. To optimize long-term operating endurance, however, strict encapsulation methods and inert processing settings are still advised [33],[36].

II.6.6 Advantages and Disadvantages and Challenges of $CsSnGeI_3$

The profile of $CsSnGeI_3$ presents a compelling dichotomy of unprecedented potential and rigorous technical hurdles [36].

a) Advantages:

- **Eco-Friendly Composition:** Eliminating hazardous lead completely reduces obstacles related to the environment and regulations. Optimal Bandgap: For optimal light harvesting, an optical bandgap of about 1.5 eV is in perfect alignment with the sun spectrum.
- **Improved Stability:** Better air and thermal stability are made possible by the synergistic coupling of inorganic Cs and Ge-alloying, which significantly delays the fast oxidation characteristic of tin-based systems.
- **High Carrier Mobility:** If defects are controlled, theoretical electron and hole mobilities indicate little bulk recombination.

b) Disadvantages :

- **Poor long-term stability under heat**, moisture, oxygen, and UV light.
- **Degradation over time**, leading to reduced efficiency.
- **Lead toxicity in most high-efficiency perovskite materials,** creating environmental concerns.
- **Sensitivity to humidity**, requiring careful encapsulation and protection.
- **Ion migration within the perovskite layer**, causing performance instability and hysteresis.
- **Interface defects and recombination losses**, which reduce device performance.

c) Challenges:

- **Defect Sensitivity:** Device efficiency is critically governed by the defect density within the absorber layer. Simulation results demonstrate that when the defect density exceeds a threshold of 10^{16} cm^{-3}, device performance deteriorates precipitously. Achieving such low defect concentrations in physical fabrication requires exquisite control over crystallization kinetics.
- **Interface Engineering:** The band alignment between $CsSnGeI_3$ and traditional transport layers (such as TiO_2) is frequently suboptimal. Mismatched energy levels result in severe interfacial recombination and large voltage deficits. Additional manufacturing complexity is introduced by the identification and deposition of alternate, matched transport layers (e.g., SnS_2 or Cu_2O).
- **Empirical Translation:** Early experimental prototypes have recorded practical PCEs in the single digits (e.g., ~7%), despite numerical models predicting efficiencies over 30%. Closing

this disparity requires intensive experimental refinement regarding film morphology and precursor stoichiometry [34].

II.7 Applications and Future Prospects of Perovskite Solar Cells

The unique blend of high efficiency, mechanical flexibility, semi-transparency, and low-cost manufacturing endows perovskite solar cells with a versatile range of applications that extend significantly beyond traditional terrestrial power generation [37],[38].

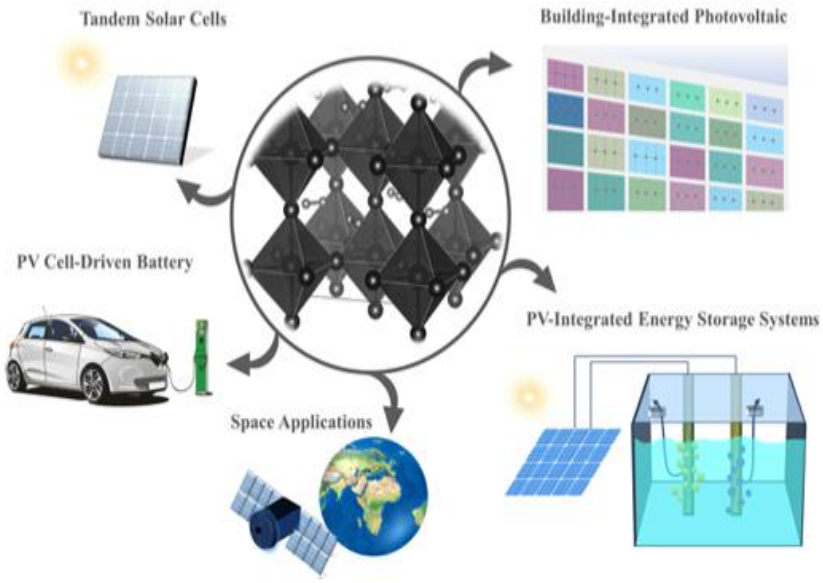


Figure (II.12): The figure outlines the development of halide perovskite materials-based applications [37].

II.7.1 Current Applications

While standalone, single-junction perovskite modules are actively being scaled up by several start-up companies, the most immediate and impactful commercial application is in tandem solar cells. By depositing a wide-band gap perovskite cell on top of a commercial silicon or CIGS bottom cell, the resulting multi-junction device can harvest the high-energy blue photons more efficiently (minimizing thermalization losses) while the bottom cell captures the low-energy red and infrared photons. Perovskite-silicon tandem cells have already surpassed 33% efficiency in laboratory settings, decisively breaking the theoretical limit of silicon alone. Furthermore, the tenable band gap and potential for semi-transparency make PSCs exceptionally suited for Building-Integrated Photovoltaics (BIPV), such as solar windows, where traditional opaque silicon panels are unviable. Their compatibility with flexible plastic

substrates also opens avenues for portable electronics, aerospace applications (owing to high power-to-weight ratios), and integration into smart textiles [39].

II.7.2 Future Developments and Research Trends

The future trajectory of perovskite photovoltaics is profoundly focused on solving the stability and scalability paradigms. Advanced manufacturing techniques, such as blade coating, slot-die coating, and vapor deposition, are being optimized to translate small-area laboratory efficiencies to large-area commercial modules without sacrificing film quality or uniformity. In terms of materials science, the paradigm is shifting heavily towards defect passivation using bulky organic spacer molecules that form 2D/3D hybrid perovskite structures. These 2D layers act as a barrier against moisture ingress and suppress ion migration, significantly bolstering long-term operational stability. Furthermore, as discussed in the context of this thesis, the aggressive development of high-performance lead-free materials, particularly through intricate compositional alloying like $CsSnGeI_3$ and the utilization of machine learning algorithms to discover novel stable phases, represents the ultimate frontier in ensuring the environmental sustainability of this technology [40].

II.8 Conclusion

In summary, perovskite solar cells constitute a revolutionary breakthrough in photovoltaic technology, merging the high-efficiency metrics of traditional crystalline inorganic semiconductors with the low-cost, versatile manufacturing of thin-film technologies. The unique properties of the ABX_3 crystal structure notably its tenable band gap, tremendous absorption coefficient, and robust defect tolerance facilitate unparalleled optoelectronic performance. Even with problems with environmental durability, sensitivity to moisture, and lead toxicity still present, intensive global research is quickly finding workable answers. A significant change is to thoroughly examine inorganic, lead-free materials such $CsSnGeI_3$ in order to strike a compromise between great energy outputs and rigorous environmental safety criteria. Perovskite solar cells are poised to play a crucial, transformative role in the future distribution of sustainable, renewable energy over the next few decades as methods for encapsulation, large-area processing, and defect passivation continue to improve.

Bibliography for Chapter II

[1] A. S. Bhalla, R. Guo, and R. Roy, "The perovskite structure - A review of its role in ceramic science and technology," *Materials Research Innovations*, vol. 4, no. 1, pp. 3–26, 2000, doi: 10.1007/S100190000062.

[2] P. Roy, A. Ghosh, F. Barclay, A. Khare, and E. Cuce, "Perovskite Solar Cells: A Review of the Recent Advances," *Coatings 2022, Vol. 12*, vol. 12, no. 8, Jul. 2022, doi: 10.3390/COATINGS12081089.

[3] M. Becker, T. Klüner, and M. Wark, "Formation of hybrid ABX3 perovskite compounds for solar cell application: first-principles calculations of effective ionic radii and determination of tolerance factors," *Dalton Transactions*, vol. 46, no. 11, pp. 3500–3509, Mar. 2017, doi: 10.1039/C6DT04796C.

[4] S. F. Hoefler, G. Trimmel, and T. Rath, "Progress on lead-free metal halide perovskites for photovoltaic applications: a review," *Monatshefte für Chemie - Chemical Monthly 2017 148:5*, vol. 148, no. 5, pp. 795–826, Mar. 2017, doi: 10.1007/S00706-017-1933-9.

[5] C. Li, X. Lu, W. Ding, L. Feng, Y. Gao, and Z. Guo, "Formability of ABX 3 (X = F, Cl, Br, I) halide perovskites," *Acta Crystallogr. B*, vol. 64, no. 6, pp. 702–707, Dec. 2008, doi: 10.1107/S0108768108032734;JOURNAL:JOURNAL:S05677408;WGROUP:STRING:PUBLICATION.

[6] K. Chen, S. Schünemann, S. Song, and H. Tüysüz, "Structural effects on optoelectronic properties of halide perovskites," *Chem. Soc. Rev.*, vol. 47, no. 18, pp. 7045–7077, Sep. 2018, doi: 10.1039/C8CS00212F.

[7] I. Mosquera-Lois, Y. T. Huang, H. Lohan, J. Ye, A. Walsh, and R. L. Z. Hoye, "Multifaceted nature of defect tolerance in halide perovskites and emerging semiconductors," *Nature Reviews Chemistry 2025 9:5*, vol. 9, no. 5, pp. 287–304, Apr. 2025, doi: 10.1038/s41570-025-00702-w.

[8] R. Brakkee and R. M. Williams, "Minimizing Defect States in Lead Halide Perovskite Solar Cell Materials," *Applied Sciences 2020, Vol. 10*, vol. 10, no. 9, Apr. 2020, doi: 10.3390/APP10093061.

[9] S. Bhattarai *et al.*, "A detailed review of perovskite solar cells: Introduction, working principle, modelling, fabrication techniques, future challenges," *Micro and Nanostructures*, vol. 172, p. 207450, Dec. 2022, doi: 10.1016/J.MICRNA.2022.207450.

[10] H. S. Jung and N. G. Park, "Perovskite solar cells: From materials to devices," *Small*, vol. 11, no. 1, pp. 10–25, Jan. 2015, doi: 10.1002/SMLL.201402767;JOURNAL:JOURNAL:16136829;PAGEGROUP:STRING:PUBLICATION.

[11] I. Hussain, H. P. Tran, J. Jaksik, J. Moore, N. Islam, and M. J. Uddin, "Functional materials, device architecture, and flexibility of perovskite solar cell," *Emergent Materials 2018 1:3*, vol. 1, no. 3, pp. 133–154, Nov. 2018, doi: 10.1007/S42247-018-0013-1.

[12] R. A. Afre and D. Pugliese, "Perovskite Solar Cells: A Review of the Latest Advances in

Materials, Fabrication Techniques, and Stability Enhancement Strategies," *Micromachines 2024, Vol. 15*, vol. 15, no. 2, Jan. 2024, doi: 10.3390/MI15020192.

[13] T. Webb, S. J. Sweeney, and W. Zhang, "Device Architecture Engineering: Progress toward Next Generation Perovskite Solar Cells," *Adv. Funct. Mater.*, vol. 31, no. 35, p. 2103121, Aug. 2021, doi: 10.1002/ADFM.202103121;REQUESTEDJOURNAL:JOURNAL:16163028;WGROUP:STRING:PUBLICATION.

[14] S. Dongmin Kang and G. Jeffrey Snyder, "Charge-transport model for conducting polymers," *Nature Materials 2016 16:2*, vol. 16, no. 2, pp. 252–257, Nov. 2016, doi: 10.1038/nmat4784.

[15] N. E. Courtier, J. M. Cave, J. M. Foster, A. B. Walker, and G. Richardson, "How transport layer properties affect perovskite solar cell performance: insights from a coupled charge transport/ion migration model," *Energy Environ. Sci.*, vol. 12, no. 1, pp. 396–409, Jan. 2019, doi: 10.1039/C8EE01576G.

[16] V. Zardetto *et al.*, "Atomic layer deposition for perovskite solar cells: research status, opportunities and challenges," *Sustain. Energy Fuels*, vol. 1, no. 1, pp. 30–55, Mar. 2017, doi: 10.1039/C6SE00076B.

[17] M. H. Miah, M. U. Khandaker, M. B. Rahman, M. Nur-E-Alam, and M. A. Islam, "Band gap tuning of perovskite solar cells for enhancing the efficiency and stability: issues and prospects," *RSC Adv.*, vol. 14, no. 23, pp. 15876–15906, May 2024, doi: 10.1039/D4RA01640H.

[18] J. De Roo *et al.*, "Highly Dynamic Ligand Binding and Light Absorption Coefficient of Cesium Lead Bromide Perovskite Nanocrystals," *ACS Nano*, vol. 10, no. 2, pp. 2071–2081, Feb. 2016, doi: 10.1021/ACSNANO.5B06295.

[19] J. Huang, Y. Yuan, Y. Shao, and Y. Yan, "Understanding the physical properties of hybrid perovskites for photovoltaic applications," *Nature Reviews Materials 2017 2:7*, vol. 2, no. 7, pp. 17042-, Jul. 2017, doi: 10.1038/natrevmats.2017.42.

[20] B. Saparov and D. B. Mitzi, "Organic–Inorganic Perovskites: Structural Versatility for Functional Materials Design," *Chem. Rev.*, vol. 116, no. 7, pp. 4558–4596, Apr. 2016, doi: 10.1021/ACS.CHEMREV.5B00715.

[21] W. Li, Z. Wang, F. Deschler, S. Gao, R. H. Friend, and A. K. Cheetham, "Chemically diverse and multifunctional hybrid organic-inorganic perovskites," *Nat. Rev. Mater.*, vol. 2, no. 3, pp. 16099-, Feb. 2017, doi: 10.1038/NATREVMATS.2016.99;SUBJMETA.

[22] L. Zhang, Y. Zhao, and Q. Dai, "Recent Progress in Perovskite Solar Cell: Fabrication, Efficiency, and Stability," *Challenges and Advances in Computational Chemistry and Physics*, vol. 32, pp. 1–32, 2021, doi: 10.1007/978-3-030-69445-6_1.

[23] J. Liang *et al.*, "All-Inorganic Perovskite Solar Cells," *J. Am. Chem. Soc.*, vol. 138, no. 49, pp. 15829–15832, Dec. 2016, doi: 10.1021/JACS.6B10227.

[24] W. Xiang and W. Tress, "Review on Recent Progress of All-Inorganic Metal Halide Perovskites and Solar Cells," *Adv. Mater.*, vol. 31, no. 44, Nov. 2019, doi: 10.1002/ADMA.201902851.

[25] J. Irvine *et al.*, "Roadmap on inorganic perovskites for energy applications," *Journal of Physics: Energy*, vol. 3, no. 3, p. 031502, Jul. 2021, doi: 10.1088/2515-7655/ABFF18.

[26] S. Nagane *et al.*, "Lead-Free Perovskite Semiconductors Based on Germanium–Tin Solid Solutions: Structural and Optoelectronic Properties," *The Journal of Physical Chemistry C*, vol. 122, no. 11, pp. 5940–5947, Mar. 2018, doi: 10.1021/ACS.JPCC.8B00480.

[27] Y. Saito *et al.*, "Lead-free piezoceramics," *Nature 2004 432:7013*, vol. 432, no. 7013, pp. 84–87, Oct. 2004, doi: 10.1038/nature03028.

[28] Y. Wang *et al.*, "Toward eco-friendly and stable halide perovskite-inspired materials for light-emitting devices applications by dimension classification: Recent advances and opportunities," *EcoMat*, vol. 4, no. 1, p. e12160, Jan. 2022, doi: 10.1002/EOM2.12160;PAGEGROUP:STRING:PUBLICATION.

[29] T. Wu *et al.*, "The Main Progress of Perovskite Solar Cells in 2020–2021," *Nano-Micro Letters 2021 13:1*, vol. 13, no. 1, pp. 152-, Jul. 2021, doi: 10.1007/S40820-021-00672-W.

[30] M. Noman, I. N. Khan, A. Qamar, K. AlSnaie, and H. M. H. Farh, "Mathematical Modeling and Optimization of Highly Efficient Nontoxic All-Inorganic CsSnGeI3-Based Perovskite Solar Cells with Oxide and Kesterite Charge Transport Layers," *ACS Omega*, vol. 9, no. 10, p. 11398, Mar. 2024, doi: 10.1021/ACSOMEGA.3C07754.

[31] A. K Al-Mousoi *et al.*, "Comparative Study of the Correlation between Diffusion Length of Charge Carriers and the Performance of CsSnGeI3 Perovskite Solar Cells," *Energy & Fuels*, vol. 36, no. 23, pp. 14403–14410, Dec. 2022, doi: 10.1021/ACS.ENERGYFUELS.2C03390.

[32] N. A.-I. J. of A. in Science and undefined 2024, "Optimization Study of Lead-Free Cssngei3 Perovskite Based Solar Cell Structures," *academia.eduH ArbouzInternational Journal of Advances in Science, Engineering and Technology, 2024•academia.edu*, Accessed: May 19, 2026. [Online]. Available: https://www.academia.edu/download/118985778/6_999_1727502825127_134.pdf

[33] M. F. Rahman, R. Akter, M. F. Hossain, N. Badi, and A. Irfan, "Unraveling a Novel CsSnI3 and CsSnGeI3 Double Absorber Perovskite Solar Cell," *Int. J. Energy Res.*, vol. 2025, no. 1, p. 1804390, Jan. 2025, doi: 10.1155/ER/1804390.

[34] H. Sabbah, "Numerical Simulation of 30% Efficient Lead-Free Perovskite CsSnGeI3-Based Solar Cells," *Materials 2022, Vol. 15*, vol. 15, no. 9, Apr. 2022, doi: 10.3390/MA15093229.

[35] T. Rikhitha, N. V. N. S. Harshitha, P. P. Dharani, D. N. Sai, and A. K. Dikshit, "Performance Modeling of a MASnI3/CsSnGeI3 Bilayer Lead-Free Perovskite Solar Cell Through SCAPS-1D," *3rd International Conference on Power Electronics and Energy, ICPEE 2025*, 2025, doi: 10.1109/ICPEE65973.2025.11410784.

[36] H. Devi, M. Sharma, V. Bharti, A. Tara, S. Sharma, and R. Gupta, "Designing High-Performance Tandem Solar Cells Using Pb-free Organic–Inorganic Perovskite Materials," *Journal of Electronic Materials 2025 54:7*, vol. 54, no. 7, pp. 5419–5437, May 2025, doi: 10.1007/S11664-025-12034-Y.

[37] A. S. R. Bati, Y. L. Zhong, P. L. Burn, M. K. Nazeeruddin, P. E. Shaw, and M. Batmunkh, "Next-generation applications for integrated perovskite solar cells," *Communications Materials 2023 4:1*, vol. 4, no. 1, pp. 2-, Jan. 2023, doi: 10.1038/s43246-022-00325-4.

[38] C. Yang *et al.*, "Achievements, challenges, and future prospects for industrialization of perovskite solar cells," *Light: Science & Applications 2024 13:1*, vol. 13, no. 1, pp. 227-, Sep. 2024, doi: 10.1038/s41377-024-01461-x.

[39] T. Leijtens, K. A. Bush, R. Prasanna, and M. D. McGehee, "Opportunities and challenges for tandem solar cells using metal halide perovskite semiconductors," *Nature Energy 2018 3:10*, vol. 3, no. 10, pp. 828–838, Jul. 2018, doi: 10.1038/s41560-018-0190-4.

[40] Y. Zhao and K. Zhu, "Organic–inorganic hybrid lead halide perovskites for optoelectronic and electronic applications," *Chem. Soc. Rev.*, vol. 45, no. 3, pp. 655–689, Feb. 2016, doi: 10.1039/C4CS00458B.

Chapter III: Results and Discussion of the C_SSnGeI_3 Perovskite Solar Cell Simulation

III.1 Introduction

This chapter is divided into two main sections. The solar cell capacitance simulator (SCAPS-1D), which is used to simulate C_SSnGeI_3 perovskite solar cells, is thoroughly described in the first section. The perovskite solar cell in the $CsSnGeI_3$ architecture and some physical characteristics, including thickness, temperature, and photovoltaic parameters used in this investigation, are described in the second section. Additionally, some results from using the SCAPS-1D program are presented and discussed in this section [1].

III.2 Presentation of the SCAPS-1D Software

We must walk through three primary windows in order to use SCAPS software to simulate and manipulate every parameter of a photovoltaic device [2]:

- The "action panel" execution window;
- The "Definition panel" window for device design and problem definition;
- The window for results.

a). "Action panel" on the main menu

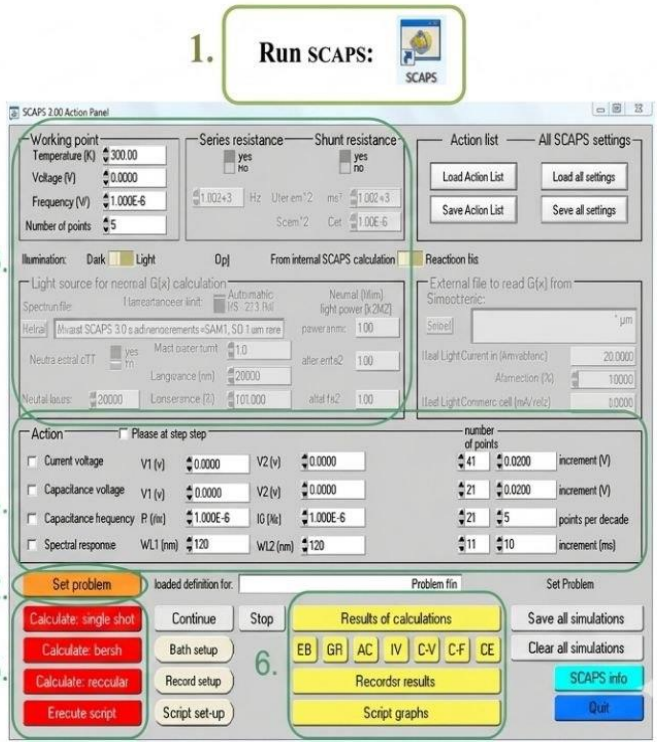
You can change the temperature, series and parallel resistance, and lighting parameters after starting the program and entering the run window (Figure III.1). As seen in the graphics below, you can visit the device design window and the results window at any moment.

b) Choosing a structure

The "SOLAR DEFINITION" panel opens when you click the "SET PROBLEM" button in the action panel. This enables you to load or save solar cell structures from other files, as well as construct or change them (Figure III. 2).

There are dedicated panels for the basic actions:

1. Run SCAPS .
2. Define the problem, thus the geometry, the materials, all properties of your solar cell
3. Indicate the circumstances in which you want to do the simulation, i.e. specify the working point
4. Indicate what you will calculate, i.e. which measurement you will simulate.
5. Start the calculation(s)
6. Display the simulated curves.



1. Run SCAPS :

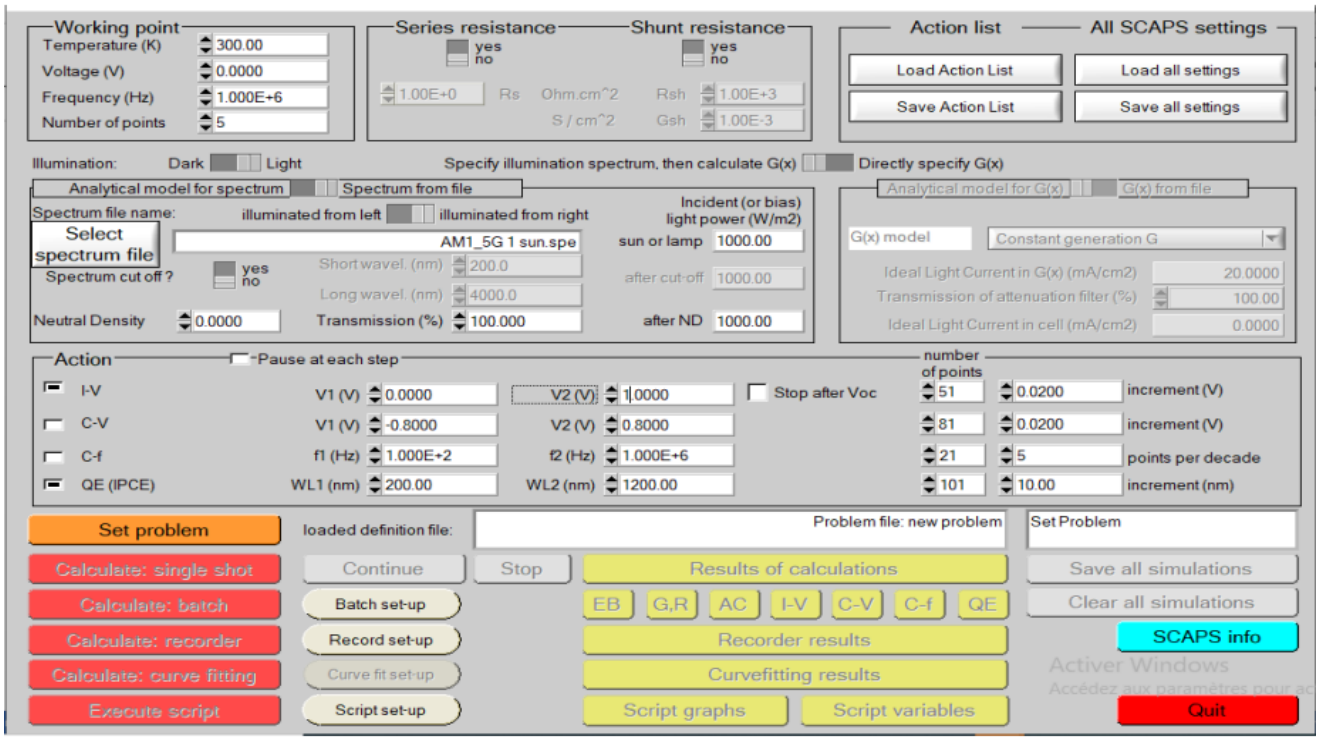


Figure (III.1): The action or main window for the SCAPS startup

2. Describe the issue, including the solar cell's geometry, materials, and other characteristics.



Figure (III.2): Solar cell structure definition.

c) Layer characteristics

The window in Figure III.3 includes parameters such as gap energy, electrical permittivity, affinity, doping, and doping type. It should be noted that standard values can be entered directly into the software's data files.

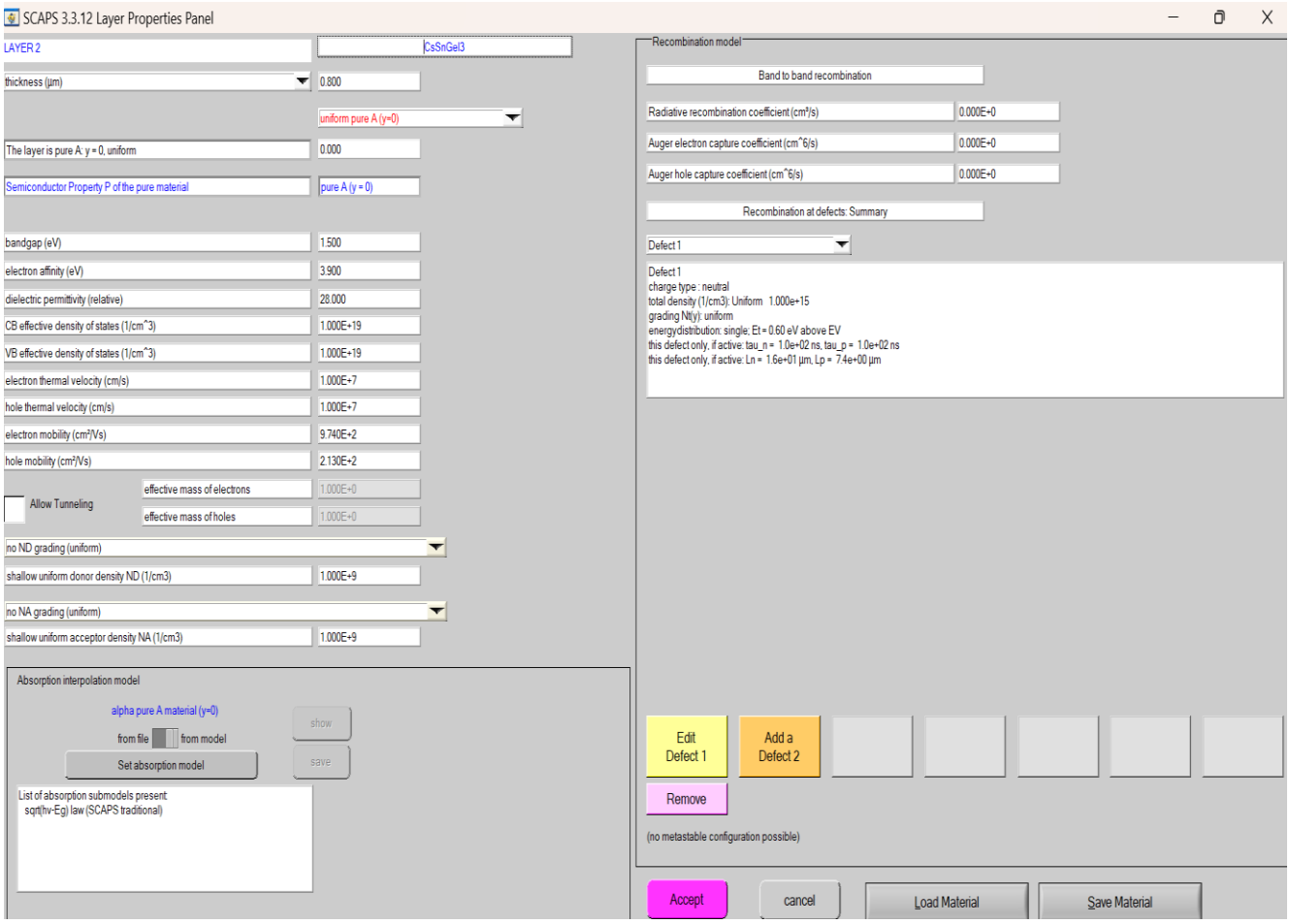


Figure (III.3): Characteristics of a CsSnGeI3 Perovskite cell layer

d) Simulation findings « Characteristic I(V)»

Run the "Calculate" simulation and record the results (Jsc, Vco, FF, η) in the "I-V panel" window, including the I-V characteristic. Pressing « show » displays and copies these findings as a table (figure III.4).

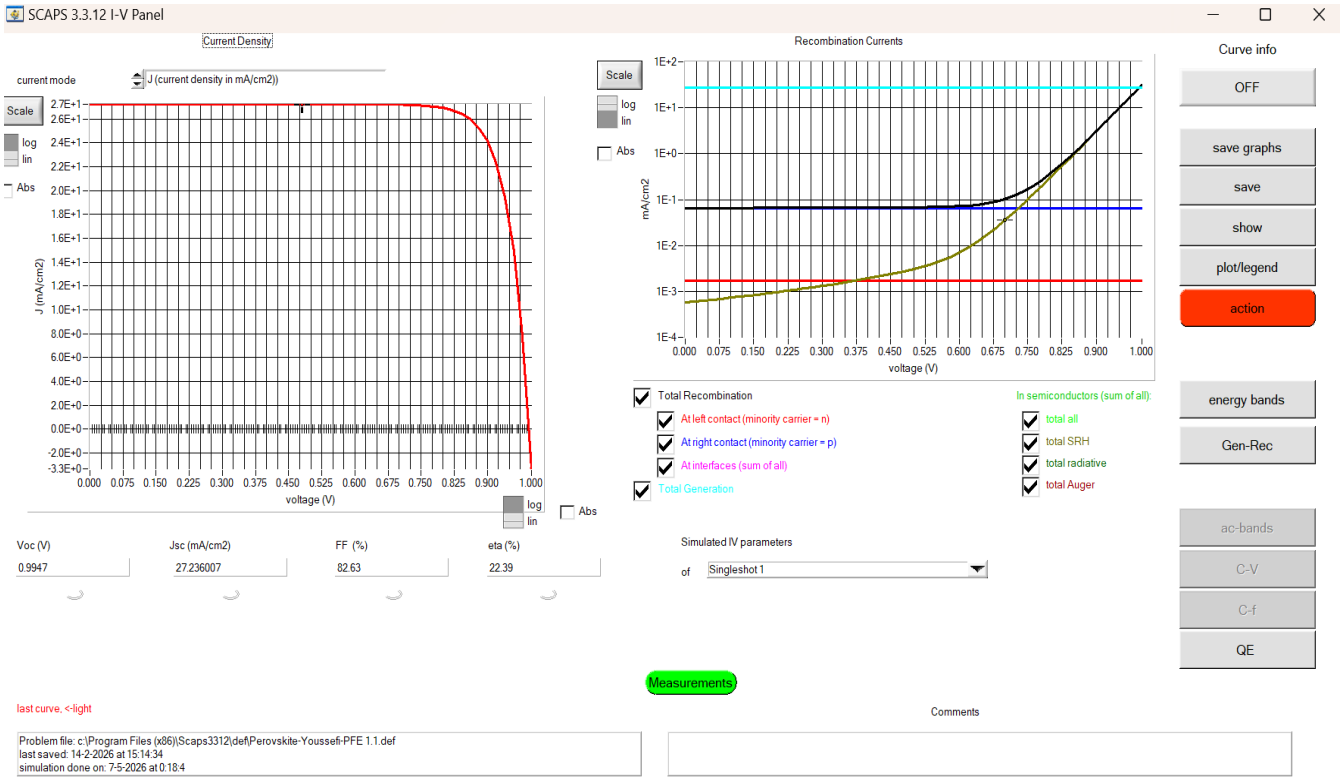


Figure (III.4): Display panel for the I-V curves

III.3 Results and Discussion

III.3.1 The Structure Studied

Our design of perovskite solar cells (PSCs), they are based on the p-i-n structure, consisting of a perovskite absorbing layer cesium tin-germanium triiodide (**$CsSnGeI_3$**) sandwiched between a hole transparent material (HTM) and an electron transparent material (ETM): **FTO/HTL/Perovskite/ETL/Au** perovskite solar cell (Figure III.5). All device performances were simulated using the air mass 1.5 solar spectra with 1000 W/cm^2 irradiance at T = 300 K.

In this arrangement, $CsSnGeI_3$ absorbs light forming electron-hole pairs. $CsSnGeI_3$ has a lower VB energy level (−5.40 eV) than Cu_2O (−5.37 eV), allowing excited holes to be transported to the Au electrode via the Cu2O layer. Electrons migrate from the $CsSnGeI_3$ layer's conduction band (CB) to the STO layer and then to the FTO, as the CB energy level of STO (-3.9 eV) is lower than that of $CsSnGeI_3$.

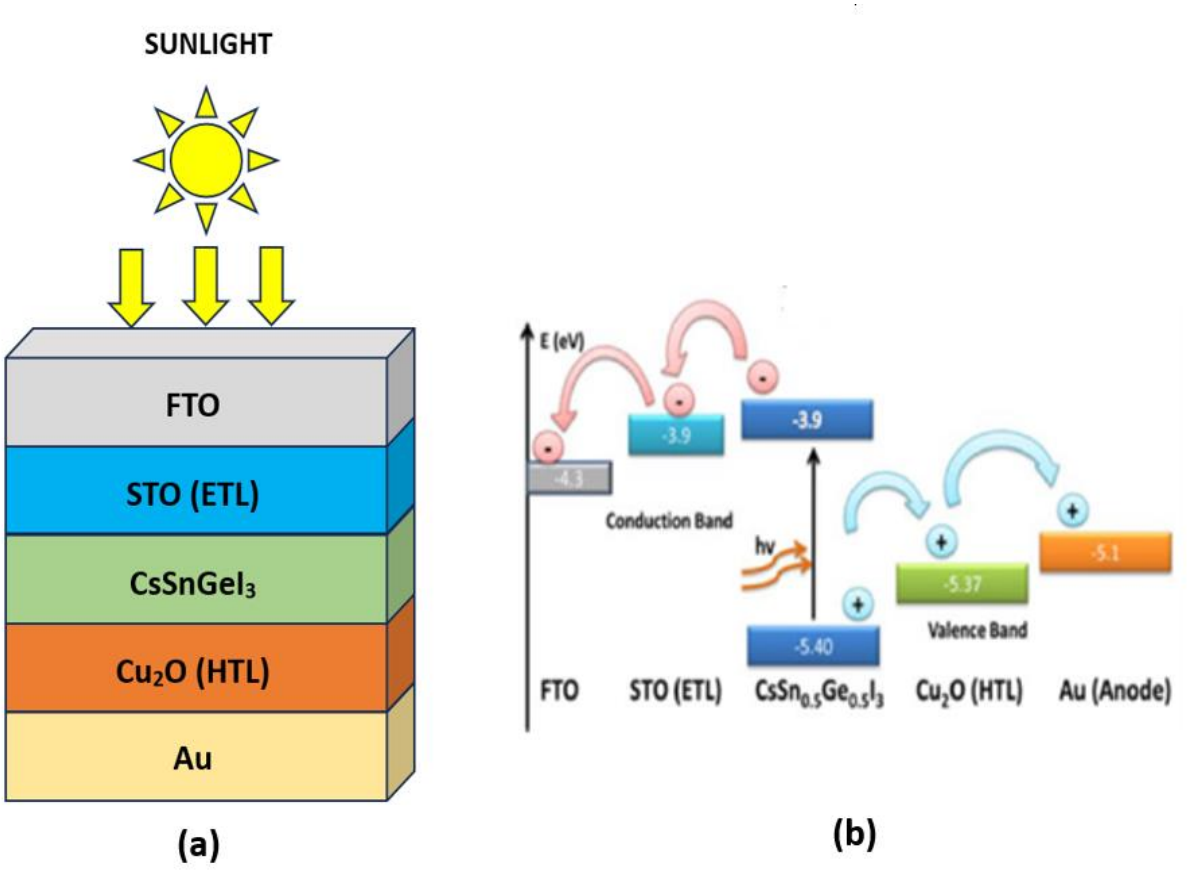


Figure (III. 5): a) $CsSnGeI_3$-based PSC structure and b) charge carrier movement [3]

SCAPS 1D software analyzes a variety of optical and electrical parameters, such as energy bands, external quantum efficiency (EQE), and I-V characteristics. This analysis was carried out by solving both a continuity equation and Poisson's equation for charge carriers.[4], [5] Equations (1) and (2) are the continuity equations., while Eq. (3) solves Poisson's Equation:

$$\nabla . J_n - q\frac{\partial n}{\partial t} = +qR \quad \text{(III.1)}$$

$$\nabla . J_n + q\frac{\partial n}{\partial t} = +qR \quad \text{(III.2)}$$

$$\nabla^2 \Psi - \frac{q}{\varepsilon}(n - p + N_a - N_d) \quad \text{(III.3)}$$

where J_n is the electron density, J_p is the hole density, R is the charge carrier recombination rate, N_A is the concentration of p-type dopants, N_D is the concentration of n-type dopants, and Ψ is the electric field potential.

The physical parameters of the various layers of the structure are summarized in the following table (Table III.1):

Table (III.1) Device parameters such as FTO, HTL, ETL, and the CSSnGeI3 absorber layer are used for PSCs configuration [14]

Parameters	FTO	STO	Cu_2O	$C_SS_nG_eI_3$
Thickness (nm)	200	70	350	800
χ (eV)	4.0	4	3.2	3.9
Eg (eV)	3.5	3.20	2.17	1.5
Ɛr	9.0	8.7	7.11	28
N_C ($1/cm^3$)	2.2E+18	1.7E+19	2.020E+17	1.0E+19
N_V ($1/cm^3$)	1.8E+19	2.0E+20	1.100E+19	1.0E+19
μ_n (cm^2/Vs)	20	5.3E+3	200	974
μ_p (cm^2/Vs)	10	6.6E+2	80	213
N_A (1/cm3)	0	0	1.00E+18	1.0E+9
N_D (1/cm3)	1.0E+18	2.0E+16	0	1.0E+9
N_t ($1/cm^3$)	1.0E+14	1.0E+14	1.0E+15	1.0E+15

III.3.2 Effect of the C_SSnGeI_3 layer thickness on the photovoltaic parameters of the solar cell

The thickness of the perovskite layer significantly impacts the performance of PSCs [6], [7]. A thicker perovskite layer absorbs lighter, increasing its thickness and usually resulting in a higher device PCE.

The electrical characteristics of perovskite solar cells were thoroughly examined in relation to the thickness of the absorbing perovskite layer, as shown in figures III.6, III.7, and III. 8. The results show a noteworthy trend: the efficiency of the solar cells rises with increasing perovskite layer thickness, reaching an ideal value before finally falling. These findings have led to the conclusion that 1000 nm is the ideal thickness for the perovskite layer.

At 1000 nm of absorber layer thickness, the optimized cell structure produced a current density Jsc = 27.72 mA/cm2, an open circuit voltage Voc = 0.9819V, a full factor FF = 82.60%, and a maximum power conversion efficiency PCE of 22.48%. The results are summarized in the following table (Table III.2):

Table (III.2). Results showing the effect of the thickness of the CSSnGeI3 absorber layer on the photovoltaic parameters of the solar cell

C_SSnGeI_3 absorber layer (µm)	Jsc (mA/cm^2)	Voc (v)	FF %	PCE %
0.2	19.78	1.0731	84.90	18.03
0.4	24.40	1.0350	83.06	20.98
0.6	26.32	1.0114	82.69	22.02
0.8	27.23	0.9947	82.63	22.39
1	**27.72**	**0.9819**	**82.60**	**22.48**
2	28.45	0.9433	82.24	22.08
3	28.62	0.9214	81.62	21.52

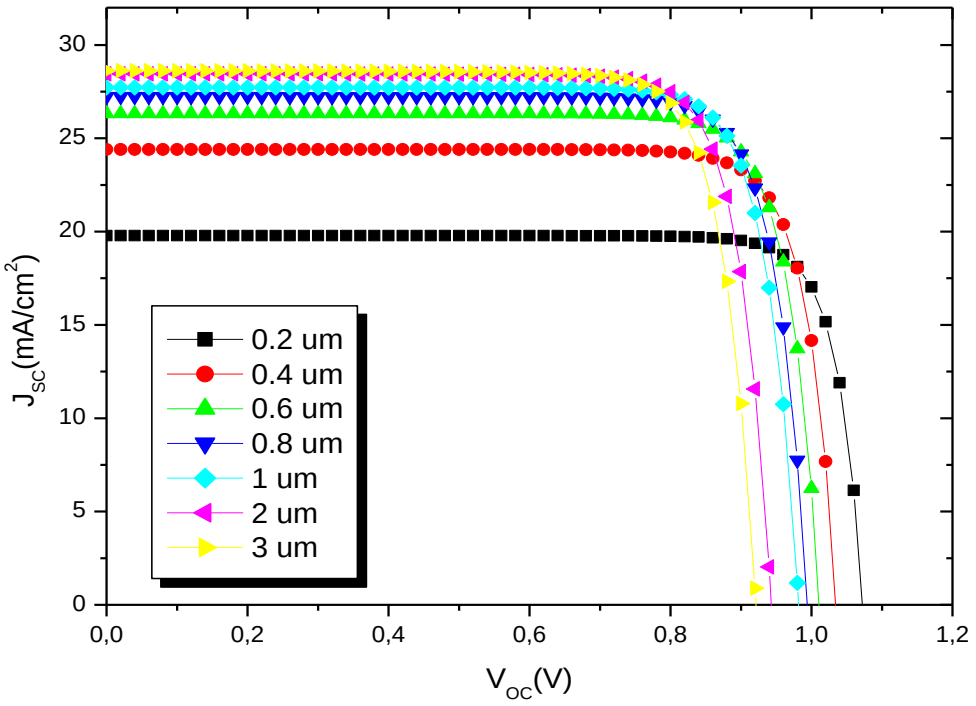


Figure (III.6) Effect of the thickness of the CSSnGeI3 absorber layer on the I-V characteristics of the solar cell

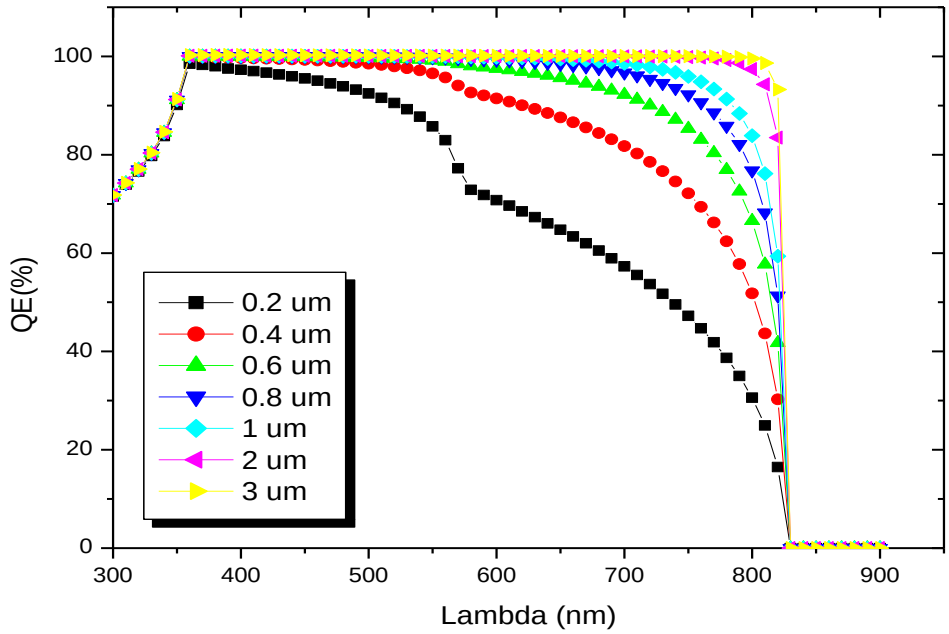


Figure (III.7): Effect of the thickness of the CSSnGeI3 absorber layer on the EQE characteristics of the solar cell

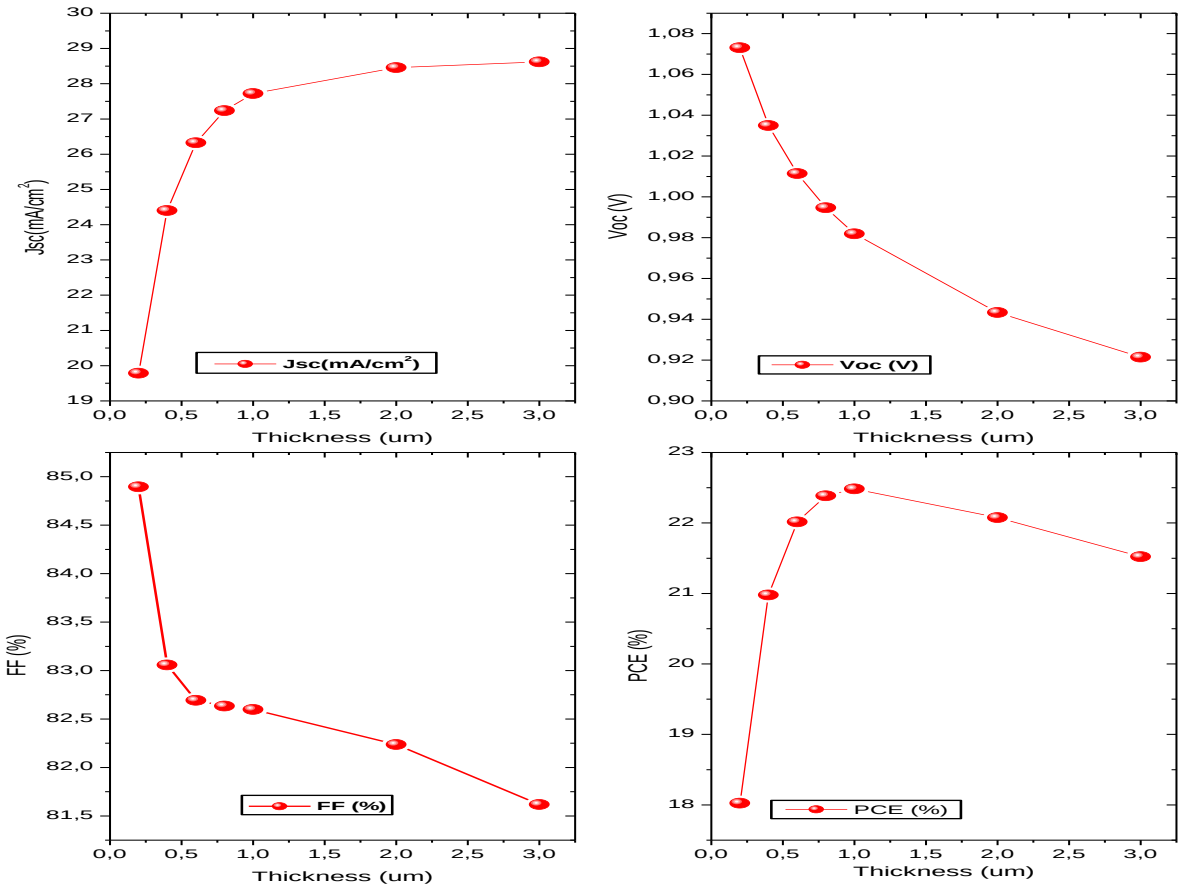


Figure (III.8): Effect of the thickness of the CSSnGeI3 layer on the photovoltaic parameters of the solar cell

III.3.3 Simulation of a perovskite solar cell using different HTL layer materials

Various HTLs, including Cu2O, CuSCN, $CuSbS_2$, Cul, CFTS, and CBTS, have been employed to enhance the performance and examine the effects of ETLs on solar cells. Table III.3 displays the performance of the different ETLs utilized in place of Cu_2O within the PSC framework.

Table (III.3) Physical properties of the various materials used in the HTL layer [14]

Parameters	Cu_2O	CuSCN	CuSbS2	Cul	CFTS	CBTS
Thickness (μm)	0.350	0.350	0.350	0.350	0.350	0.350
Eg (eV)	2.171	3.4	1.580	2.980	1.3	1.9
χ (eV)	3.2	1.9	4.2	2.1	3.3	3.6
εr	7.110	9	8.2	6.5	9	5.4
μ_n $(cm^2/V.\,s)$	2.0×10^{2}	1.0×10^{-4}	20	20	2.198×10^{1}	30
μ_p $(cm^2/V.\,s)$	8.0×10^{1}	1.0×10^{-1}	10	10	2.198×10^{1}	10
Effective density of states at CB (cm^{-3})	2.02×10^{17}	2.2×10^{18}	2×10^{18}	1×10^{22}	2.2×10^{18}	2.2×10^{18}
Effective density of states at VB (cm^{-3})	1.8×10^{19}	2.9×10^{19}	1×10^{19}	1×10^{22}	1.9×10^{19}	1.8×10^{19}
Density of Nd donors (cm^{-3})	0	0	0	0	0	0
Density of Na acceptors (cm^{-3})	1.0×10^{18}	1.0×10^{18}	1.380×10^{18}	2.0×10^{18}	1×10^{18}	1×10^{18}
Density of defects Nt (cm^{-3})	1.0×10^{15}	1.0×10^{14}	1.0×10^{14}	1.0×10^{14}	1.0×10^{15}	1.0×10^{14}

The J-V characteristic curve was derived from the simulation of the data presented in Table III.3 for various HTL layers. Figure III.9 illustrates that $CuSbS_2$ yields more optimized results than other HTL layers due to its an efficient absorption layer (lower transmittance) in solar cells compared to all HTL layers [8]. The output parameters of the PSC obtained using different HTL layers are presented in Table III. 4. The Jsc value for $CuSbS_2$ HTL was found to be **27.4482** mA/cm², and $CuSbS_2$ HTL-based PSC exhibited the highest PCE of **22.61**% among all other HTLs, indicating that $CuSbS_2$ can be a suitable alternative for the HTL layer [8] .

The quantum efficiency of a perovskite solar cell is the amount of current produced when it is exposed to photons of a particular wavelength. The quantum efficiency curve of the perovskite solar cell is shown in Figure III.10 for different hole transport layers within the wavelength range of 300–830 nm. The QE values exceed 98%. Quantum efficiency increases with increasing wavelength from 350 to 400 nm before remaining almost constant up to 700 nm. The QE gradually decreases up to 830 nm. The $CuSbS_2$ QE curve is nearly indistinguishable from those of all HTL layers, indicating that $CuSbS_2$ has potential as a solar cell absorption

material [8].

Table (III.4). Effects of different HTL layer materials on the photovoltaic performance of perovskite solar cells.

HTL	Cu_2O	CuSCN	$CuSbS_2$	CuI	CFTS	CBTS
Voc (v)	0.9947	0.9888	**0.9974**	0.9954	0.8777	0.9964
Jsc(mA/cm2)	27.2360	27.2277	**27.4482**	27.2312	30.6755	27.2559
FF (%)	82.63	82.61	**82.57**	79.23	57.14	82.64
PCE (%)	22.39	22.24	**22.61**	21.47	15.38	22.44

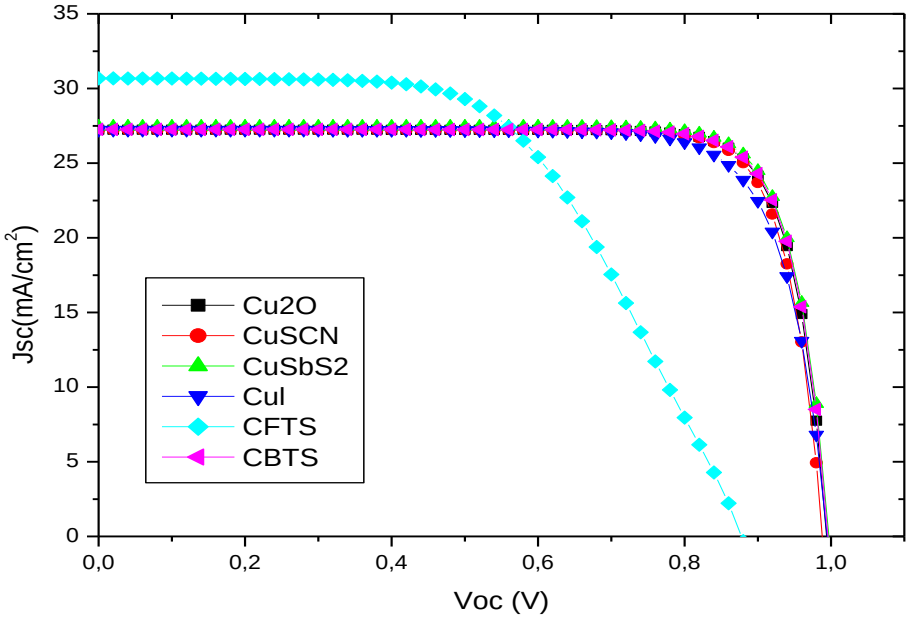


Figure (III.9) Influence of different HTL layer materials on the I-V characteristics of the solar cell

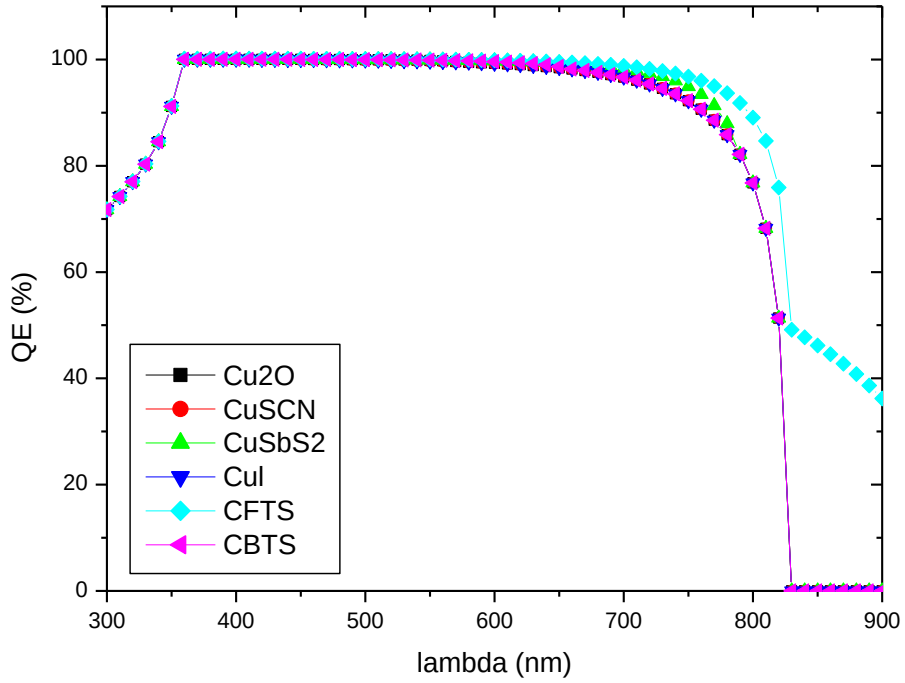


Figure (III.10) Influence of different HTL layer materials on the EQE characteristics of the solar cell

III.3.4 Simulation of a perovskite solar cell using different ETL layer materials

Several ETLs, such as TiO_2, ZnO, PCBM, C_{60}, and ZnSe, have been used to optimize the performance to investigate the impacts of ETLs on the performance of solar cells. Table III.5 shows the performance of the various ETLs that have been used in place of STO in the structure of PSC.

Table (III.5): Physical Parameters of the Different Materials of the ETL Layer [14]

Parameters	STO	C60	TiO2	ZnO	PCBM	ZnSe
Thickness (μm)	0.070	0.070	0.070	0.070	0.070	0.070
Eg (eV)	3.2	1.7	3.2	3.3	2	2.810
χ (eV)	2	3.9	4	4	3.9	4.090
εr	8.7	4.2	9	9	3.9	8.6
μ_n $(cm^2/V.\,s)$	5.3×10^{3}	8.0×10^{-2}	20	100	0.2	1.1×10^{2}
μ_p $(cm^2/V.\,s)$	6.6×10^{2}	3.5×10^{-3}	10	25	0.2	4.0×10^{2}
Effective density of states at CB (cm^{-3})	1.7×10^{19}	8.0×10^{19}	2.0×10^{18}	3.7×10^{18}	2.5×10^{21}	2.2×10^{18}
Effective density of states at VB (cm^{-3})	2.0×10^{20}	8.0×10^{19}	1.8×10^{19}	1.8×10^{19}	2.5×10^{21}	1.8×10^{19}
Density of Nd donors (cm^{-3})	2.0×10^{16}	1.0×10^{17}	9.0×10^{16}	1.0×10^{18}	2.93×10^{17}	1.0×10^{18}
Density of Na acceptors (cm^{-3})	0	0	0	0	0	0
Density of defects Nt (cm^{-3})	1.0×10^{15}	1.0×10^{15}	1.0×10^{15}	1.0×10^{15}	1.0×10^{15}	1.0×10^{15}

The J-V characteristic curve was derived from the simulation of the data presented in Table III.5 for various ETL layers. Figure III.11 illustrates that ZnO yields more optimized results than other ETL layers due to its superior conductivity and transmittance[9]. The output parameters of the PSC obtained using different ETLs are presented in Table III. 6. The Jsc value for ZnO ETL was found to be 27.232 mA/cm², and ZnO ETL-based PSC exhibited the highest PCE of 22.83% among all other ETLs, indicating that ZnO can be a suitable alternative for the ETL layer[9].

The quantum efficiency of a perovskite solar cell is the amount of current generated when it is exposed to photons of a specific wavelength. Figure III.12 shows the QE curve of the PSC for different ETL layers within the wavelength range of 300–830 nm. The QE values are greater than 98%. The quantum efficiency increases with increasing wavelength from 350 to 400 nm, and then remains almost constant up to 700 nm. The QE gradually decreases up to 830 nm. The ZnO QE curve is almost identical to that of all ETL layers except for C60, thereby offering a new, cost-effective alternative for the ETL layer that is easy to fabricate [10].

Table (III.6). Results of the perovskite solar cell with different ETL layer materials on

ETL	STO	ZnO	C60	PCBM	TiO2	ZnSe
Voc (v)	0.9947	**1.0039**	0.9933	0.9934	0.9992	0.9967
Jsc(mA/cm2)	27.236	**27.232**	24.593	27.152	27.233	27.234
FF (%)	82.63	**83.52**	80.37	83.17	83.43	83.44
PCE (%)	22.39	**22.83**	19.63	22.43	22.70	22.65

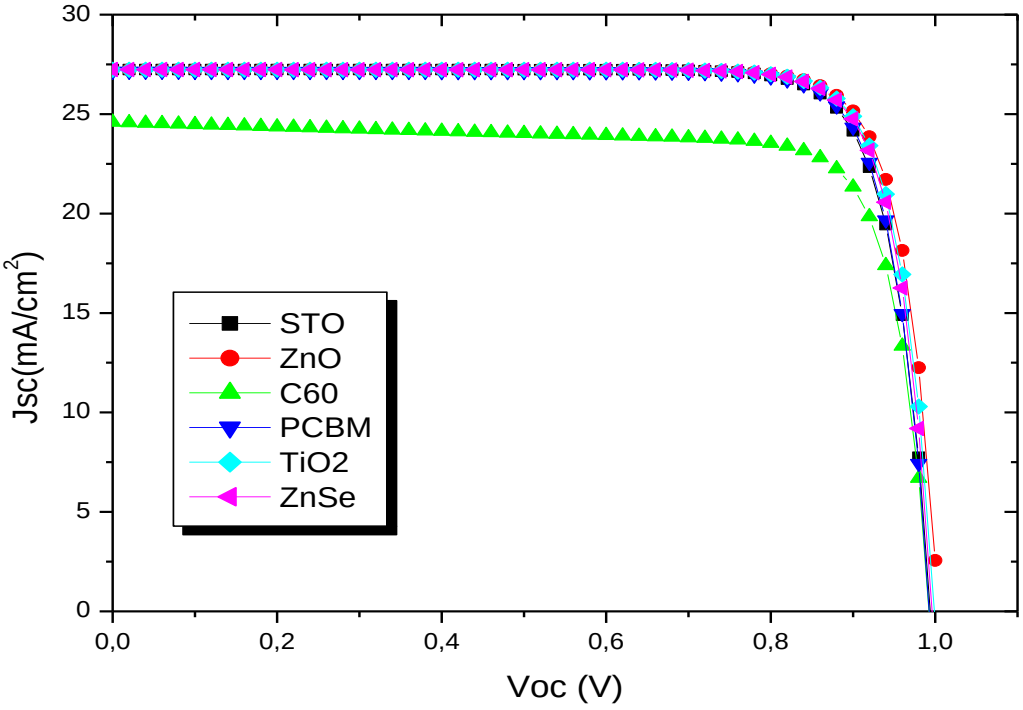


Figure (III.11) Influence of different ETL layer materials on the I-V characteristics of the solar cell

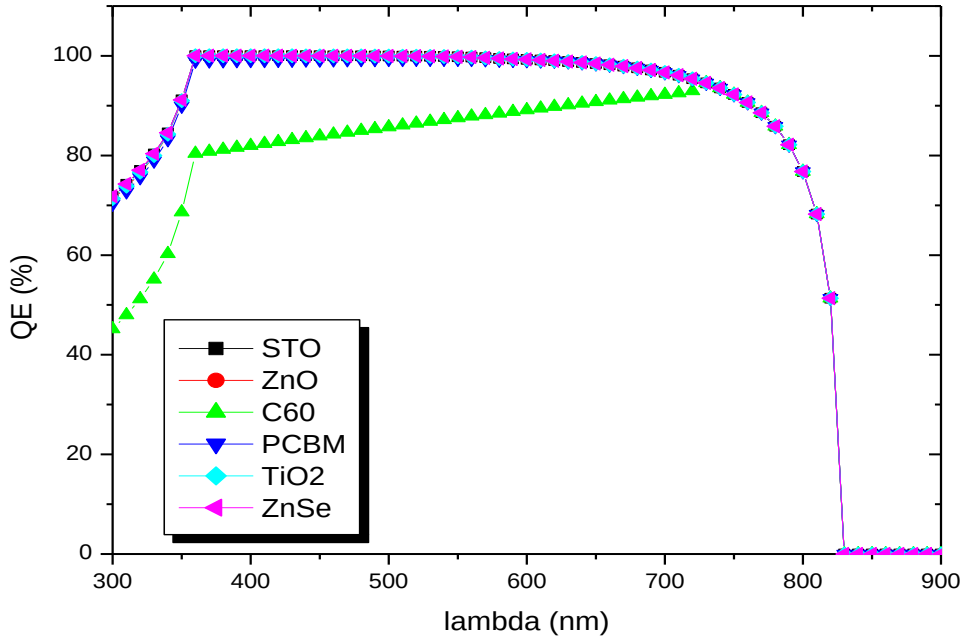


Figure (III.12) Influence of different ETL layer materials on the EQE characteristic of the solar cell

III.3.5 Effect of temperature on the photovoltaics parameters solar cell

The performance of a device is significantly impacted by its operating temperature. The suggested cell performance has been investigated at different temperatures to provide light on the effect. By maintaining the same other values, the simulated temperature will rise from 300 to 450 K. The results from Figure III.13 and Figure III.14 confirm that as J_{SC} rises, other parameters including *FF*, *Voc*, and *PCE* fall as the temperature rises. The increasing trend in *Jsc* with increased temperature is also caused by a decrease in energy bandgap, which generates more charge carriers[11].

From 300K to 450K, the J_{SC} increased from 27,2360 mA/cm2 to 27,2486 mA/cm2, but the V_{OC} decreased to 0,68488V from 0,99467V. Along with FF falling to 71.21% from 82.63% in Figure III.14, the temperature changes also caused a significant efficiency loss of about 40%. This decline is explained by the impact of temperature on a number of material characteristics, such as absorption coefficients, bandgap, and electron and hole transport[12]. These modifications to the material's characteristics may cause the cell's resistance to rise, which would lower its PCE [13].

Table (III.7). Results of the effects of temperature variations (300–450 K) on the photovoltaic parameters of a perovskite solar cell

T(°K)	300	330	360	390	420	450
Voc (v)	0,99467	0,93356	0,87197	0,80997	0,74759	0,68488
Jsc(mA/cm2)	27,2360	27,2381	27,2405	27,2434	27,2463	27,2486
FF (%)	82,6340	80,7015	78,6197	76,3556	73,8888	71,2154
PCE (%)	22,38624	20,52123	18,6745	16,8489	15,0505	13,2903

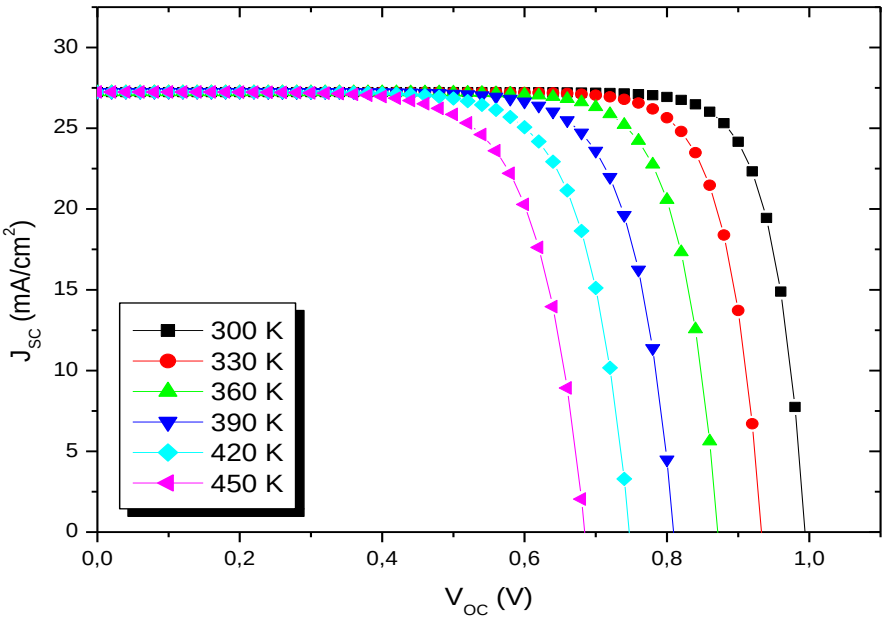


Figure (III.13) Effect of temperature on the I-V characteristics of solar cell

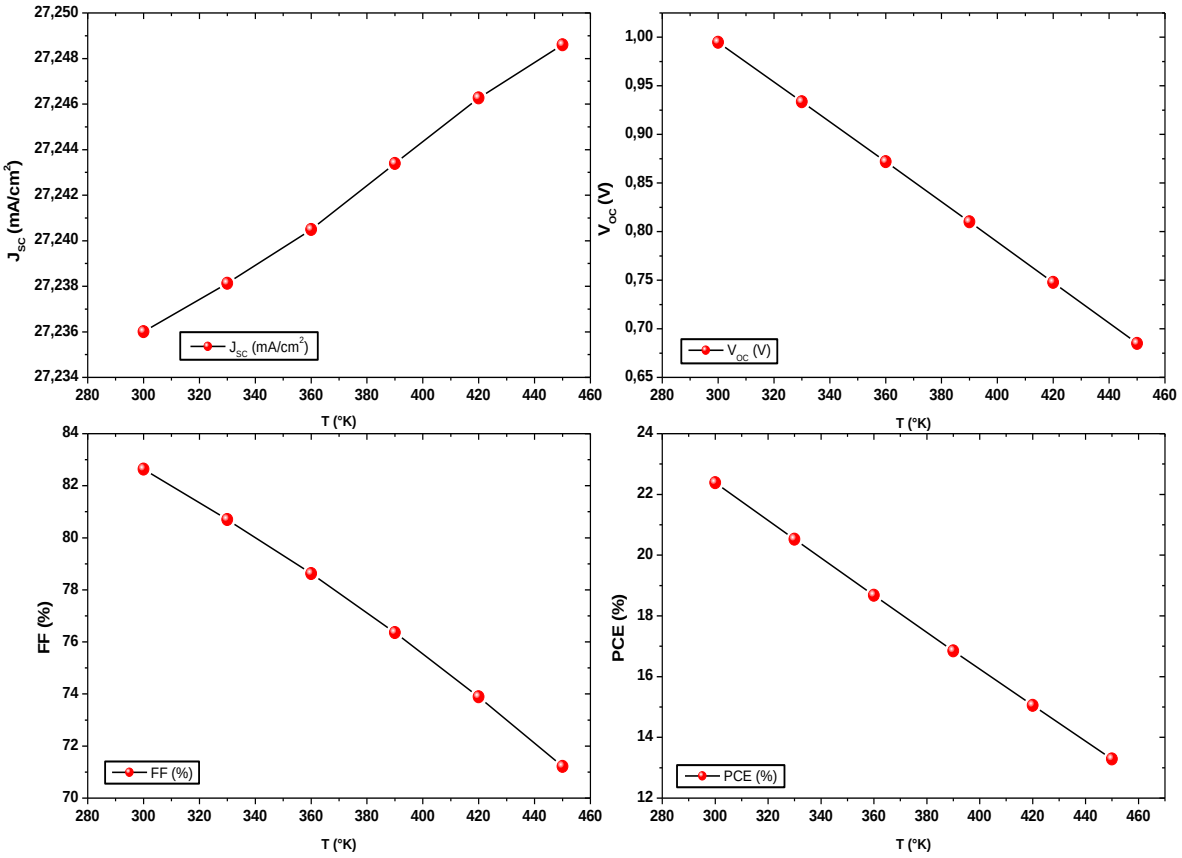


Figure (III.14) Effect of temperature on the photovoltaïques parameters solar cell

III.4 Conclusion

This chapter presented a detailed SCAPS-1D simulation of a lead-free CsSnGeI3 perovskite solar cell and assessed how its structure and operating conditions influence photovoltaic performance. The initial **FTO/HTL/CsSnGeI3/ETL/Au** configuration, using **Cu2O** and **STO** as transport layers, already showed strong potential, reaching a power conversion efficiency of **22.39%.** A thickness study confirmed that absorber dimensions play a critical role:
layers that are too thin reduce light absorption, while overly thick layers intensify recombination losses. The best balance was obtained at about **1000 nm**, where the efficiency increased to **22.48%**. Temperature analysis further showed that device performance declines markedly as heat rises, mainly because higher temperatures strengthen recombination and lower the open-circuit voltage, highlighting the need for effective thermal control. A comparative optimization of charge transport layers then identified CuSbS2 as the most suitable hole transport material and **ZnO** as the most effective electron transport material. With these interface layers, the simulated efficiency improved to **22.83%**. Overall, the results confirm that CsSnGeI3 is a promising, stable, and environmentally safer absorber for high-performance lead-free perovskite solar cells, while the optimized parameters obtained here provide a solid basis for future experimental fabrication and further interface engineering studies.

Bibliography for Chapter III

[1] M. L. BENYAHIA, "Study and simulation of Photovoltaic Properties on the Performance of p-InGaN/n-InGaN Single Junction. Numerical simulation," Memoire, AMAR TELIDJI UNIVERSITY- LAGHOUAT, Laghouat, 2024.

[2] M. Burgelman, K. Decock, A. Niemegeers, J. Verschraegen, and S. Degrave, "SCAPS manual," *users.elis.ugent.beM Burgelman, K Decock, A Niemegeers, J Verschraegen, S DegraveUniversity of Ghent: Ghent, Belgium, 2016•users.elis.ugent.be*, Accessed: May 07, 2026. [Online]. Available: https://users.elis.ugent.be/ELISgroups/solar/projects/scaps/SCAPS%20manual%20most%20recent.pdf

[3] H. Devi, M. Sharma, V. Bharti, A. Tara, S. Sharma, and R. Gupta, "Designing High-Performance Tandem Solar Cells Using Pb-free Organic–Inorganic Perovskite Materials," *SpringerH Devi, M Sharma, V Bharti, A Tara, S Sharma, R GuptaJournal of Electronic Materials, 2025•Springer*, vol. 54, no. 7, pp. 5419–5437, Jul. 2025, doi: 10.1007/S11664-025-12034-Y.

[4] Q. Duan *et al.*, "Design of hole-transport-material free CH3NH3PbI3/CsSnI3 all-perovskite heterojunction efficient solar cells by device simulation," *Solar Energy*, vol. 201, pp. 555–560, May 2020, doi: 10.1016/J.SOLENER.2020.03.037.

[5] Y. Raoui, H. Ez-Zahraouy, N. Tahiri, O. El Bounagui, S. Ahmad, and S. Kazim, "Performance analysis of MAPbI3 based perovskite solar cells employing diverse charge selective contacts: Simulation study," *Solar Energy*, vol. 193, pp. 948–955, Nov. 2019, doi: 10.1016/J.SOLENER.2019.10.009.

[6] A. Tara, V. Bharti, S. Sharma, and R. Gupta, "Device simulation of FASnI3 based perovskite solar cell with Zn(O0.3, S0.7) as electron transport layer using SCAPS-1D," *Opt. Mater. (Amst).*, vol. 119, p. 111362, Sep. 2021, doi: 10.1016/J.OPTMAT.2021.111362.

[7] D. Y. Son, J. H. Im, H. S. Kim, and N. G. Park, "11% Efficient Perovskite Solar Cell Based on ZnO Nanorods: An Effective Charge Collection System," *Journal of Physical Chemistry C*, vol. 118, no. 30, pp. 16567–16573, Jul. 2014, doi: 10.1021/JP412407J.

[8] N. Shu, Q. H.-C. Lett, and undefined 2016, "Studies on structural, optical and electrical properties of CuSbS2 nanoparticles," *chalcogen.roB Shu, Q HanChalcogenide Lett, 2016•chalcogen.ro*, vol. 13, no. 2, pp. 46–53, 2016, Accessed: May 07, 2026. [Online]. Available: https://www.chalcogen.ro/46_Shu.pdf

[9] S. Stojadinović, D. Pjević, and N. Radić, "Photocatalytic Properties of ZnO/WO3 Coatings Formed by Plasma Electrolytic Oxidation of a Zinc Substrate in a Tungsten-Containing Electrolyte," *Coatings 2025, Vol. 15*, vol. 15, no. 6, May 2025, doi: 10.3390/COATINGS15060657.

[10] H. Simchi, B. E. McCandless, T. Meng, and W. N. Shafarman, "Structural, optical, and surface properties of WO3 thin films for solar cells," *J. Alloys Compd.*, vol. 617, pp. 609–615, Dec. 2014, doi: 10.1016/J.JALLCOM.2014.08.047.

[11] V. Srivastava, R. K. Chauhan, and P. Lohia, "Lead Free Perovskite Solar Cell Using TiO2 as an Electron Transport Materials and Cu2O as a Hole Transport Materials," *Lecture Notes in Electrical Engineering*, vol. 911, pp. 305–311, 2022, doi: 10.1007/978-981-19-2631-0_28/SAVE-RESEARCH.

[12] K. Fatema and M. S. Arefin, "Enhancing the efficiency of Pb-based and Sn-based perovskite solar cell by applying different ETL and HTL using SCAPS-ID," *Opt. Mater. (Amst).*, vol. 125, p. 112036, Mar. 2022, doi: 10.1016/J.OPTMAT.2022.112036.

[13] N. T.-Int. J. E. P. Eng and undefined 2021, "Numerical analysis of CsSnGeI3 perovskite solar cells using SCAPS-1D," *academia.eduT ThomasInt. J. Energy Power Eng, 2021•academia.edu*, Accessed: May 07, 2026. [Online]. Available: https://www.academia.edu/download/97901885/10.11648.j.ijepe.20211005.12.pdf

[14] Hossain, M. K., Toki, G. I., Kuddus, A., Rubel, M. H. K., Hossain, M. M., Bencherif, H., & Mushtaq, M. (2023). An extensive study on multiple ETL and HTL layers to design and simulation of high-performance lead-free CsSnCl3-based perovskite solar cells. Sci. Rep. 13 (1), 2521 (2023).

General conclusion:

At the end of this work, it can be concluded that photovoltaic energy is one of the most relevant solutions for meeting current energy challenges while reducing the environmental impact of conventional sources. In this context, perovskite solar cells have attracted increasing scientific interest because of their remarkable optoelectronic properties, strong light absorption, tunable bandgap, and potential for low-cost fabrication. This study linked the theoretical foundations of photovoltaics with the opportunities offered by leadfree perovskites in order to support the development of devices that are more efficient, more stable, and more environmentally friendly.

The theoretical review first showed that the operation of a photovoltaic cell is based on light absorption, the generation of electron-hole pairs, and their separation and collection inside the device. The comparison of the different generations of solar cells also highlighted that, despite the industrial dominance of silicon, new technologies are still needed to overcome limitations related to fabrication cost, energy-intensive processes, and material constraints. In this regard, perovskite solar cells stand out as a promising pathway capable of combining high efficiency with relatively simple architectures.

This thesis then focused on lead-free inorganic perovskites in order to address the major issues of toxicity and instability that still limit large-scale application. The choice of the $CsSnGeI_3$ material proved especially relevant because it replaces lead with a tin-germanium combination while preserving properties favorable to photovoltaic conversion. The results presented in this work indicate that this compound has a bandgap close to the ideal value for solar absorption, together with good optical absorption capability, making it a serious candidate for safer and greener solar-cell design. A major contribution of this work lies in the numerical study of the FTO/HTL/ $CsSnGeI_3$/ETL/Au structure using the SCAPS-1D software. The simulations showed that the absorber-layer thickness strongly affects cell performance, with an optimal value close to 1000 nm. They also allowed the comparison of several transport materials and identified $CuSbS_2$ as the best hole transport layer and ZnO as the best electron transport layer. Under this optimized configuration, the device reached a theoretical efficiency of about 22.83%, confirming the strong potential of this lead-free architecture. However, the study also revealed some important limitations. Rising temperature causes a noticeable drop in performance, especially in opencircuit voltage and overall efficiency. In addition, defects in the active layers or at the interfaces increase carrier recombination and reduce cell effectiveness. These findings show that, despite the promising simulated results, further efforts are still

required in thermal stability, defect passivation, interface engineering, and experimental validation. In conclusion, this thesis confirms that lead-free perovskite solar cells based on $CsSnGeI_3$ represent a highly promising research direction for the future of photovoltaics. Optimizing materials, transport layers, and structural parameters makes it possible to envision high-efficiency devices that better satisfy current environmental requirements. This work therefore provides a useful basis for future experimental studies aimed at developing solar cells that are more stable, more durable, and better suited to next-generation solar applications.